



Locoregional hyperthermia of deep-seated tumours applied with capacitive and radiative systems: a simulation study

H. P. Kok, F. Navarro, L. Strigari, M. Cavagnaro & J. Crezee

To cite this article: H. P. Kok, F. Navarro, L. Strigari, M. Cavagnaro & J. Crezee (2018) Locoregional hyperthermia of deep-seated tumours applied with capacitive and radiative systems: a simulation study, *International Journal of Hyperthermia*, 34:6, 714-730, DOI: [10.1080/02656736.2018.1448119](https://doi.org/10.1080/02656736.2018.1448119)

To link to this article: <https://doi.org/10.1080/02656736.2018.1448119>



© 2018 The Author(s). Published by Informa UK Limited, trading as Taylor & Francis Group.



Accepted author version posted online: 06 Mar 2018.
Published online: 18 Apr 2018.



Submit your article to this journal [↗](#)



Article views: 229



View Crossmark data [↗](#)

Locoregional hyperthermia of deep-seated tumours applied with capacitive and radiative systems: a simulation study

H. P. Kok^a, F. Navarro^b, L. Strigari^c, M. Cavagnaro^d  and J. Crezee^a 

^aDepartment of Radiation Oncology, Academic Medical Center, University of Amsterdam, Amsterdam, The Netherlands; ^bDepartment of Medical Physics, Regional University Hospital of Málaga, Malaga, Spain; ^cLaboratory of Medical Physics and Expert Systems, Regina Elena National Cancer Institute, Rome, Italy; ^dDepartment of Information Engineering, Electronics and Telecommunications, Sapienza University of Rome, Rome, Italy

ABSTRACT

Background: Locoregional hyperthermia is applied to deep-seated tumours in the pelvic region. Two very different heating techniques are often applied: capacitive and radiative heating. In this paper, numerical simulations are applied to compare the performance of both techniques in heating of deep-seated tumours.

Methods: Phantom simulations were performed for small ($30 \times 20 \times 50 \text{ cm}^3$) and large ($45 \times 30 \times 50 \text{ cm}^3$), homogeneous fatless and inhomogeneous fat-muscle, tissue-equivalent phantoms with a central or eccentric target region. Radiative heating was simulated with the 70 MHz AMC-4 system and capacitive heating was simulated at 13.56 MHz. Simulations were performed for small fatless, small (i.e. fat layer typically $<2 \text{ cm}$) and large (i.e. fat layer typically $>3 \text{ cm}$) patients with cervix, prostate, bladder and rectum cancer. Temperature distributions were simulated using constant hyperthermic-level perfusion values with tissue constraints of 44°C and compared for both heating techniques.

Results: For the small homogeneous phantom, similar target heating was predicted with radiative and capacitive heating. For the large homogeneous phantom, most effective target heating was predicted with capacitive heating. For inhomogeneous phantoms, hot spots in the fat layer limit adequate capacitive heating, and simulated target temperatures with radiative heating were $2\text{--}4^\circ\text{C}$ higher. Patient simulations predicted therapeutic target temperatures with capacitive heating for fatless patients, but radiative heating was more robust for all tumour sites and patient sizes, yielding target temperatures $1\text{--}3^\circ\text{C}$ higher than those predicted for capacitive heating.

Conclusion: Generally, radiative locoregional heating yields more favourable simulated temperature distributions for deep-seated pelvic tumours, compared with capacitive heating. Therapeutic temperatures are predicted for capacitive heating in patients with (almost) no fat.

ARTICLE HISTORY

Received 5 October 2017
Revised 26 February 2018
Accepted 27 February 2018
Published online 18 April 2018

KEYWORDS

Locoregional hyperthermia; RF heating; capacitive heating; hyperthermia treatment planning

Introduction

Hyperthermia, i.e. heating of tumours to temperatures of $40\text{--}43^\circ\text{C}$ for 1 h, is clinically applied to enhance the effectiveness of radiotherapy and chemotherapy [1]. Locoregional hyperthermia is applied to tumours located deeper than 4 cm beyond the skin. Clinical applications of locoregional hyperthermia involve mainly pelvic tumours, such as prostate, bladder, rectum and cervix/vagina [2–8].

The sensitisation by hyperthermia and thus the increase in clinical outcome is determined by the achieved temperatures in the target region [3,5,9]. A thermal dose–effect relationship has been demonstrated in pre-clinical and clinical studies, so it is important to aim for high tumour temperatures, with 43°C being the widely accepted goal for tumour temperatures [10].

The heating technique used can have an impact on the tumour temperatures that can be realised. Both capacitive and electromagnetic radiative hyperthermia systems are

frequently used in clinical hyperthermia for deep-seated tumours [2,3,5,11–15]. Capacitive systems were initially mainly used in Asian countries, but popularity in the Western world is increasing, since capacitive systems are more affordable and easier to use than radiative systems. Commercially available capacitive systems operating at 13.56 MHz are Oncotherm (Oncotherm Kft, Budapest, Hungary), Celsius TCS (Celsius42 + GmbH, Cologne, Germany), HY-DEEP 600 WM (Andromedic srl, Velletri, Italy) and Synchrotherm (Synchrotherm, Vigevano, Italy). The Thermotron RF8 system (Yamamoto Vinita Co, Osaka, Japan) operates at 8 MHz. Capacitive heating applies electrodes with an integrated water bolus bag. Additional boluses (overlay boluses) can be used for more aggressive skin cooling [16]. The patient is typically lying on a treatment table with an embedded electrode and integrated water bolus. Another electrode (with integrated water bolus) is positioned on the patient and the resulting currents produced by capacitive coupling with the

CONTACT H. P. Kok  H.P.Kok@amc.uva.nl  Department of Radiation Oncology, Academic Medical Center, University of Amsterdam, Meibergdreef 9, 1105 AZ Amsterdam, Netherlands

© 2018 The Author(s). Published by Informa UK Limited, trading as Taylor & Francis Group.
This is an Open Access article distributed under the terms of the Creative Commons Attribution-NonCommercial-NoDerivatives License (<http://creativecommons.org/licenses/by-nc-nd/4.0/>), which permits non-commercial re-use, distribution, and reproduction in any medium, provided the original work is properly cited, and is not altered, transformed, or built upon in any way.

human body cause heating. Synchrotherm and HY-DEEP 600 WM apply two flexible electrodes that can be positioned at any desired location on the patient. When equally sized electrodes are used, the absorbed power is directed towards the centre of the distance between the electrodes [17]. When different sizes of electrodes are combined, the power distribution is directed to the side of the smallest electrode [17]. Thus, for eccentric tumours the diameters are usually different, with the smallest electrode closest to the tumour location. Radiative external antennas induce an electromagnetic field that is coupled into the patient using a water bolus. Adequate target heating can be realised by using phase and amplitude steering to create constructive interference among the electromagnetic fields radiated by the individual antennas [18–20]. Radiative heating systems typically operate in the frequency range between 70 and 120 MHz. Examples of commercial radiative locoregional systems are the BSD-2000 systems (Pyrexar Medical, Salt Lake City, UT) [19,21] and the ALBA 4D system (ALBA Hyperthermia, Rome, Italy). The latter is similar to the 70 MHz AMC-4 system, developed and built by the Academic Medical Center Amsterdam [22].

The frequent clinical application of two distinctly different heating techniques raises the question whether there are differences in heating effectiveness between capacitive and radiative systems that lead to clinically relevant differences in heating quality for the general patient population. Evaluation of such differences by analysis of clinical studies is very difficult since 3D temperature information during clinical hyperthermia is lacking. Additionally, there is an inter-patient variation, which makes such an evaluation more complicated. For example, there can be a significant difference in average body dimensions of the patients in various clinical studies, which makes it difficult to draw conclusions about the heating effectiveness of two different techniques. Performing alternating treatment sessions with capacitive heating and radiative heating would be an option [23], but in that case institutes should have access to both types of equipment and experienced staff for both techniques. This makes a fair clinical comparison very difficult.

Therefore, a comparison of heating systems using theoretical methods would be the answer [24]. Hyperthermia treatment planning is a very useful method to analyse the differences between different heating techniques, using numerical simulation of 3D power and temperature distributions [25]. A clear advantage of a simulation study is also the direct comparison, since all variables can be kept constant in the model and only the heating system is varied. Kok *et al.* demonstrated the use of hyperthermia treatment planning to assess the impact of aperture size and operating frequency for waveguide systems [20,26]. Paulsen *et al.* evaluated the effect of the number of antennas and the operating frequency for various target locations [18]. Wust *et al.* compared the heating characteristics of the BSD Sigma-60 with four paired dipole antennas with the BSD Sigma-Eye system with 12 paired dipoles [19]. Some simulation studies have been published to compare capacitive and radiative heating. Kok *et al.* compared capacitive and radiative heating for superficial locations and large extremity lesions [27–29], while Kroeze *et al.* evaluated the differences for locoregional heating evaluating phantom

set-ups and a single patient anatomy [30]. However, a thorough theoretical evaluation of differences in heating patterns for locoregional hyperthermia with radiative and capacitive systems is not provided by the previous studies. This requires to evaluate the differences in heatability between different target locations (central and eccentric) and different patient dimensions by comparing simulated temperature distributions for common pelvic tumours.

This study applied hyperthermia treatment planning to analyse the differences in target heating between capacitive and radiative locoregional hyperthermia for deep-seated tumours. Simulations with both heating techniques were performed for small and large fatless homogeneous and inhomogeneous fat-muscle phantoms with a central or eccentric target location, assuming constant hyperthermic-level perfusion values. Additionally, heating with radiative and capacitive systems was simulated and compared for small (i.e. slender) fatless, small (i.e. fat layer typically <2 cm) and large (i.e. overweight/obese, fat layer typically >3 cm) patients with cervix, prostate, bladder or rectum tumours. The quality of the simulated target heating was quantified in terms of tumour temperatures that could be realised without overheating normal tissue.

Methods

Simulations were performed using our in-house developed hyperthermia treatment planning software, Plan2Heat, which uses voxel-based finite difference calculations [31]. Validations of the software for applications similar to the work described in this paper have been reported earlier [31,32]. The resolution applied for all simulations was $2.5 \times 2.5 \times 2.5 \text{ mm}^3$. The definitions of the radiative heating system, electrodes and water boluses were generated using the Generic Object Format [33].

Radiative and capacitive heating systems

The AMC-4 phased array system was modelled to represent radiative heating devices [22]. This system consists of four rectangular waveguides operating at 70 MHz. Phases and amplitudes of the individual antennas can be adapted to focus heating to the target region. Water bolus cooling with circulating deionised water at 12 °C was simulated to avoid overheating of the skin, similar to clinical practice [34]. A typical (minimum) bolus thickness of 5 cm was assumed.

For capacitive heating systems, different sizes of electrodes are available, varying between 4 and 30 cm in diameter [17,35–39]. When two different sizes of electrodes are applied, the heating is focussed towards the smaller electrode. The modelled electrode combinations had diameters of 25 and 25 cm, 20 and 25 cm or 15 and 25 cm, respectively, and an operating frequency of 13.56 MHz was assumed. For the electrode bolus filling circulating saline (0.4% NaCl [17,32]) or distilled water were modelled. Some clinics combine saline boluses with an overlay bolus for more aggressive cooling [14,40,41]. Different clinically used bolus temperatures for capacitive heating were modelled: a saline electrode bolus at

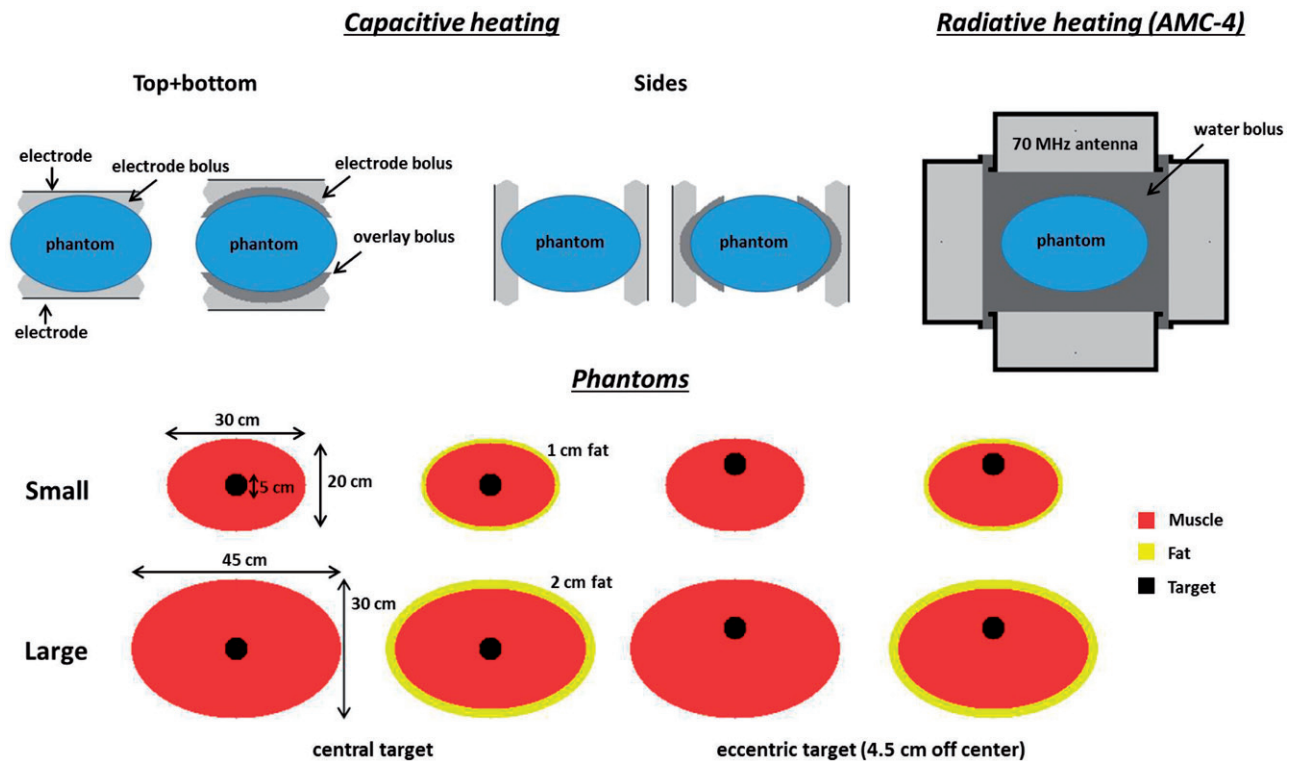


Figure 1. Schematic representation of the capacitive and radiative heating systems and the phantoms used in the simulations. The AMC-4 system consists of four rectangular waveguides, which were positioned around the phantom. Capacitive electrodes were positioned at the top and bottom of the phantom, at the sides, or alternatingly at the top and bottom and at the sides.

10 °C or 0 °C, a distilled water electrode bolus at 10 °C or 0 °C and a saline electrode bolus combined with an overlay bolus at 0 °C [17,40]. The simulated salinity for the combination with an overlay bolus was based on the study of Kato [16]. A typical thickness of the electrode bolus and overlay bolus of 1.5 cm and 2.5 cm was assumed, respectively [30]. A schematic rendition of the heating systems is shown in Figure 1.

Phantom simulations

Phantom simulations were performed for four different perfused models to analyse the basic heating properties of radiative and capacitive hyperthermia systems (see Figure 1):

- Small homogeneous phantom: a fatless cylindrical muscle-equivalent phantom with dimensions $30 \times 20 \times 50 \text{ cm}^3$.
- Large homogeneous phantom: a fatless cylindrical muscle-equivalent phantom with dimensions $45 \times 30 \times 50 \text{ cm}^3$.
- Small inhomogeneous phantom: a cylindrical fat-muscle phantom with dimensions $30 \times 20 \times 50 \text{ cm}^3$. The thickness of the fat layer is 1 cm.
- Large inhomogeneous phantom: a cylindrical fat-muscle phantom with dimensions $45 \times 30 \times 50 \text{ cm}^3$. The thickness of the fat layer is 2 cm.

For all phantoms, a central and eccentric spherical target volume with a diameter of 5 cm was modelled. The eccentric location was shifted 4.5 cm towards the top compared with the central target, which is representative for the typical eccentric location of bladder and rectum tumours. This allows

to compare the basic heating characteristics for small and large anatomies and highlights differences in heating principles when tissue heterogeneities are present.

For capacitive heating, the two electrodes were modelled positioned at the top and bottom as well as at the sides of the phantoms, to determine differences in heating effectiveness. To minimise excessive heating of normal tissue the strategy of switching the electrode positions from top + bottom to left + right was also investigated. The best possible heating that could theoretically be achieved with this switching was simulated by assuming a continuous short duty cycle (e.g. 30 s). Thermal simulations for this situation therefore assumed the power distribution to be the average of the power distribution generated by electrodes at the top + bottom and left + right, combined with continuous bolus cooling at all four sides of the phantom.

Another commonly used strategy to reduce superficial hot spots during capacitive heating is precooling before the start of the treatment. The effect of 15 min precooling with saline water boluses at 10 °C on hot spot occurrence and target heating was evaluated for the small inhomogeneous phantom.

Patient simulations

Patient simulations were performed for the most common pelvic tumour locations for which locoregional hyperthermia is applied: cervix, prostate, bladder and rectum. Small (i.e. slender) fatless, small and large (i.e. overweight/obese) patient models were derived from standard clinical CT data sets, scanned in the past 2 years. Scans should have been

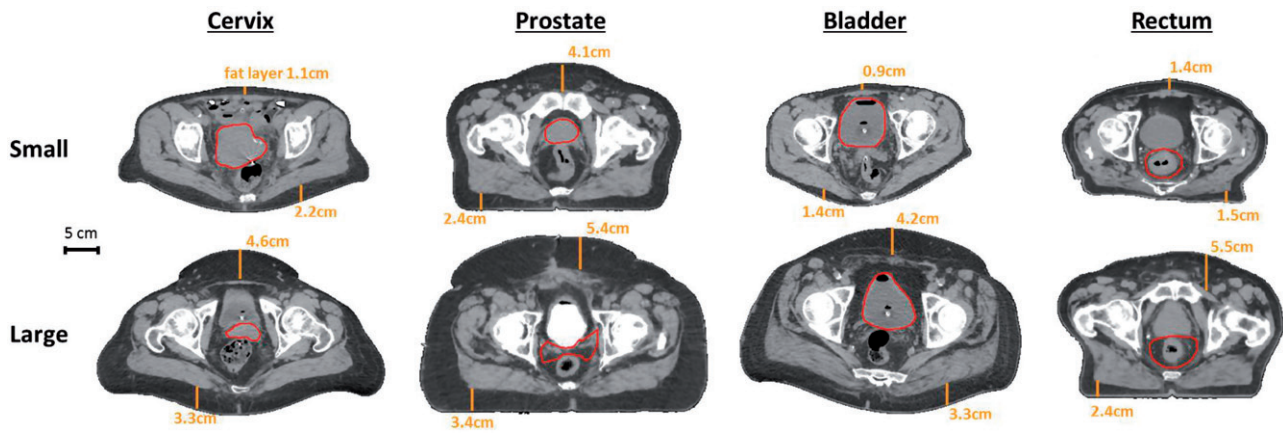


Figure 2. Transversal cross-sections of the CT scans for small (i.e. slender) and large (i.e. overweight/obese) cervix, prostate, bladder and rectum cancer patients. The scans of the cervix and bladder cancer patients were standard hyperthermia treatment planning scans for heating with the AMC-4 system, scanned in treatment position, i.e. on a water bolus and mattress. The prostate and rectum cancer patients were not treated with the AMC-4 system and standard radiotherapy scans were used, recorded on the table of the linear accelerator. Measured fat layer thicknesses are indicated and the red contour represents the target region. Cross-sections are at the centre of the target region in axial direction.

made in supine position and should be free of severe artefacts. For each tumour site, the patient with the thinnest fat layer and a patient with a large fat layer (>3 cm) were selected. Figure 2 shows transversal slices of the selected CT scans at the centre of the tumour. Fat layers were measured in anterior posterior direction in the slices at the centre of the tumour. For the small patients, the maximum fat layers were as follows: cervix 1.1–2.2 cm, prostate 2.4–4.1 cm, bladder 0.9–1.4 cm, rectum 1.4–1.5 cm, and for the large patients maximum fat layers were as follows: cervix 3.3–4.6 cm, prostate 3.4–5.4 cm, bladder 3.3–4.2 cm, rectum 2.4–5.5 cm (Figure 2). The bladder cancer patients had a full bladder, since these were treated with hyperthermia and intravesical mitomycin C. Tissue segmentation was performed using Hounsfield unit thresholds [42], distinguishing muscle, fat, bone and air. The small fatless patient model was created from the small patient model by replacing all fat tissue with muscle tissue. Contrast regions and other small artefacts, if present, were corrected manually. The tumour/target volume was delineated manually by a physician. Then the anatomy was combined with the model of the AMC-4 system or the capacitive electrodes and boluses.

SAR calculations

For radiative heating, the electromagnetic field was calculated by solving Maxwell's equations using the finite difference time domain (FDTD) method [43]. A perfectly matched layer boundary condition was applied [44]. From the electric field vector (\vec{E}), the power density (PD) or specific absorption rate (SAR) can be calculated using

$$PD = \frac{\sigma}{2} \|\vec{E}\|^2 = \rho \cdot SAR \quad (1)$$

with σ ($S m^{-1}$) the electrical conductivity and ρ ($kg m^{-3}$) the tissue density.

Because of the low frequency applied for capacitive heating, power distributions were calculated by solving the

Table 1. Values of the dielectric properties at 13.56 MHz and 70 MHz used in the simulations [46]; conductivity (σ [$S m^{-1}$]) and relative permittivity (ϵ_r [–]).

	13.56 MHz		70 MHz	
	σ ($S m^{-1}$)	ϵ_r (–)	σ ($S m^{-1}$)	ϵ_r (–)
Air	0	1	0	1
Bone	0.05	30.6	0.06	16.4
Fat	0.03	11.8	0.04	6.4
Fat (target)	0.03	11.8	0.04	6.4
Muscle	0.63	138.4	0.69	70.8
Muscle (target)	0.63	138.4	0.69	70.8
Water (distilled, 0 °C)	9.4e-5	87.7	–	–
Water (distilled, 10 °C)	6.4e-5	83.8	–	–
Water (distilled, 12 °C)	–	–	1.6e-3	83.0
Water (saline, 0.4% NaCl, 0 °C)	0.39	86.2	–	–
Water (saline, 0.4% NaCl, 10 °C)	0.51	82.4	–	–
Water (saline, comb. overlay, 0 °C)	3.0	73.5	–	–
Water (overlay bolus, 0 °C)	0.45	78.6	–	–

quasi-static formulation of Maxwell's equations. Kroeze *et al.* demonstrated that this is a valid approach for treatment planning for capacitive hyperthermia [32]. The electric field vector can be written as $\vec{E} = -\nabla V$. This quasi-static formulation yields an elliptic partial differential equation to be solved for the potential V [45]. The electrode plates at the top and bottom were kept at a constant potential of 1 V and –1 V, respectively. The boundaries of the simulation domain were fixed at zero potential. The dielectric properties used for the simulations were taken from the literature [46,47] (Table 1) and were considered constant, since the variation of dielectric properties with temperature in the range between 37 °C and 44 °C is small [48]. Some literature suggests that the electrical conductivity of human tumours could be about 10% higher than the conductivity of normal tissue [49,50]. To evaluate the possible effect of such a contrast in tissue properties on the heating effectiveness, patient simulations as described above were compared with simulations with a 10% increase in electrical conductivity for the target region compared with the values listed in Table 1.

Table 2. Values of the density and thermal properties used in the simulations [47]; density (ρ [kg m^{-3}]), specific heat capacity (c [$\text{J kg}^{-1} \text{ }^\circ\text{C}^{-1}$]), thermal conductivity (k [$\text{W m}^{-1} \text{ }^\circ\text{C}^{-1}$]) and perfusion (W_b [$\text{kg m}^{-3} \text{ s}^{-1}$]).

	ρ (kg m^{-3})	c ($\text{J kg}^{-1} \text{ }^\circ\text{C}^{-1}$)	k ($\text{W m}^{-1} \text{ }^\circ\text{C}^{-1}$)	W_b ($\text{kg m}^{-3} \text{ s}^{-1}$)
Air	1.29	1000	0.024	0
Bone	1908	1313	0.32	0.12
Fat	911	2348	0.21	1.1
Fat (target)	911	2348	0.21	1.1
Muscle	1090	3421	0.49	3.6
Muscle (target)	1090	3421	0.49	1.8
Water (distilled, 0 °C)	1000	4180	6.0	–
Water (distilled, 10 °C)	1000	4180	6.0	–
Water (distilled, 12 °C)	1000	4180	0.6	–
Water (saline, 0.4% NaCl, 0 °C)	1000	4180	6.0	–
Water (saline, 0.4% NaCl, 10 °C)	1000	4180	6.0	–
Water (saline, comb. overlay, 0 °C)	1000	4180	6.0	–
Water (overlay bolus, 0 °C)	1000	4180	6.0	–

Temperature calculations

Thermal simulations were performed by solving Pennes' bio heat equation [51]:

$$c\rho \frac{\partial T}{\partial t} = \nabla \cdot (k_{tis} \nabla T) - c_b W_b (T - T_{art}) + PD \quad (2)$$

with c the specific heat capacity ($\text{J kg}^{-1} \text{ }^\circ\text{C}^{-1}$). The first term on the right hand side represents the heat conduction in tissue, with k_{tis} ($\text{W m}^{-1} \text{ }^\circ\text{C}^{-1}$) the thermal conductivity. The second term models the perfusion, with c_b the specific heat capacity of blood, W_b ($\text{kg m}^{-3} \text{ s}^{-1}$) the volumetric perfusion rate and T_{art} the local arterial or body core temperature. Density and thermal properties were taken from the literature and are listed in Table 2 [46,47]. The initial temperature for all phantom and patient simulations was 37 °C. Constant hyperthermic-level perfusion values were assumed and constant temperature boundary conditions were applied outside the phantom or patient. An effective conductivity for the water boluses was modelled to account for the fluid dynamics [52].

For capacitive heating, steady state temperatures were calculated with the total absorbed power for each individual situation scaled such that the maximum temperature was 44 °C. For radiative heating with the AMC-4 system, steady state temperature-based phase amplitude optimisation was performed, in which the temperature at least achieved in 90% of the target (i.e. T_{90}) was maximised with constraints of 44 °C to normal tissue.

Analysis

For the phantom models, simulated temperature distributions were compared for radiative and capacitive heating. Differences in heating effectiveness for homogeneous and inhomogeneous situations were analysed as well as the impact of bolus filling, bolus temperature, precooling and switching electrode positions in the case of capacitive heating. The simulated temperature distributions were compared quantitatively by means of the indexed temperature T_{90} , which is correlated to clinical outcome [5,53]. The indexed temperature T_{90} is defined as the temperature at least achieved in 90% of the target volume. Additionally, the

simulated total absorbed power in the phantom and the target were compared.

For the patient models, the simulated temperature distributions were compared for both heating techniques. Differences in simulated heating effectiveness for small and large patients were analysed for each tumour site and quantified by the simulated target T_{10} , T_{50} and T_{90} and the total power absorbed in the patient and the target region. Definitions of T_{10} and T_{50} are analogous to the definition of T_{90} .

Results

Phantom simulations

Homogeneous phantoms

Figure 3 compares heating of a small and large homogeneous muscle-equivalent phantom with the AMC-4 system and with capacitive electrodes positioned at the top and bottom of the phantom, at the sides, or alternately at the top and bottom and at the sides. For a fair comparison between electrodes positioned at the top and bottom, at the sides or alternately, both electrodes had a diameter of 25 cm. The simulated T_{90} for a central or eccentric target location is shown. The maximum temperature in the phantom is 44 °C for all cases. Optimized antenna settings for the AMC-4 system are listed in Table 3. Simulated target temperatures decrease with increasing dimensions of the phantom for both heating techniques, because of the increasing distance of the antennas/electrodes to the target. For capacitive heating, a saline electrode bolus yields a better performance than a bolus with distilled water, with differences up to 0.6 °C for standard heating using top and bottom electrodes. More aggressive cooling at 0 °C instead of 10 °C slightly improves target heating up to 0.2 °C. The use of a saline electrode bolus in combination with an overlay bolus is optimal for capacitive heating and can increase target temperatures with ~ 1.5 °C compared with a saline electrode bolus alone. For the small phantom, the predicted temperatures for radiative and capacitive heating were comparable (~ 42 °C) and the maximum temperature of 44 °C is in the target, so heating is not limited by hot spots. For the large homogeneous phantom, capacitive heating shows up to ~ 2 °C higher predicted target temperatures than the radiative AMC-4 system.

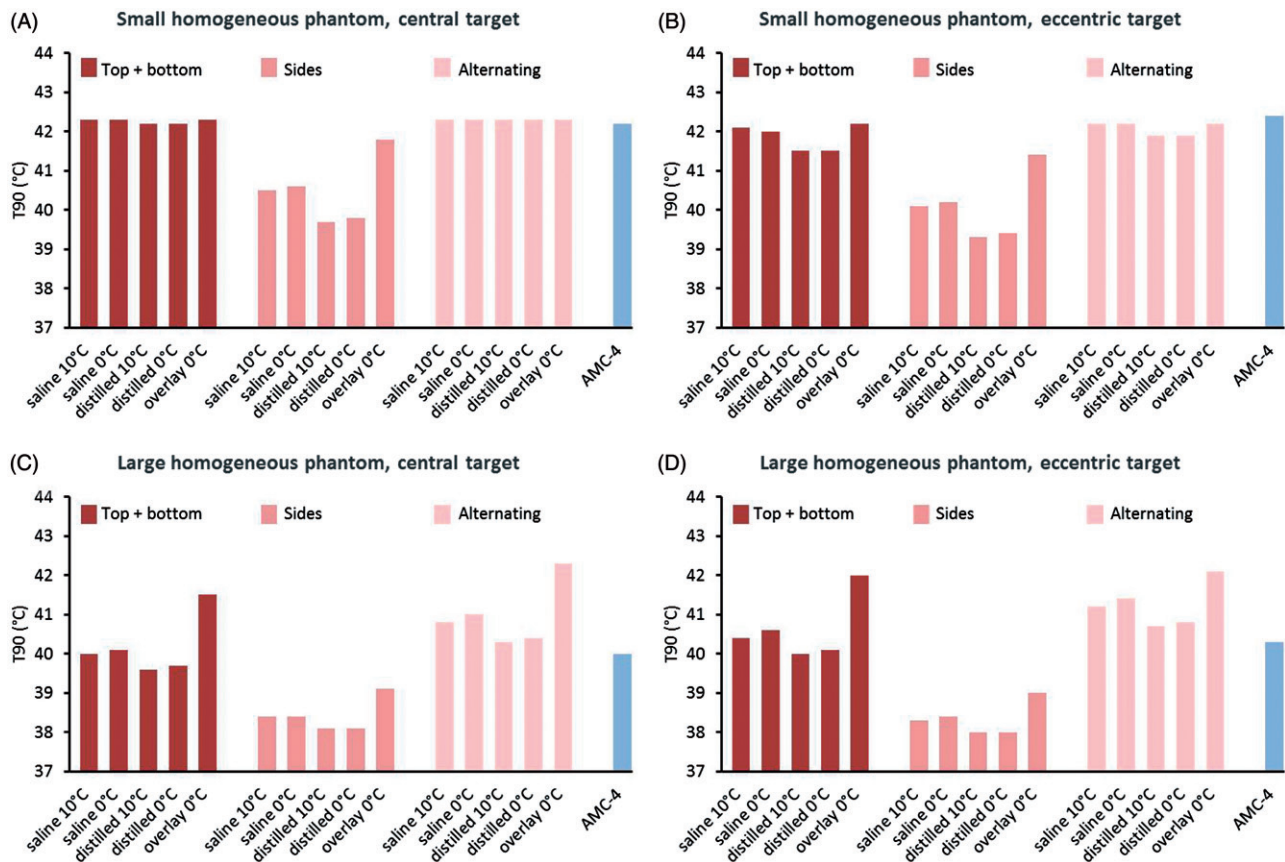


Figure 3. Simulated T_{90} target temperatures for small (A + B) and large (C + D) homogeneous phantoms, with a central or eccentric target volume, heated by two 25 cm diameter capacitive electrodes with different boluses (saline, distilled water, saline + overlay bolus) or the radiative AMC-4 system. Capacitive electrodes were positioned at the top and bottom of the phantom, at the sides or alternatingly.

Table 3. Power contribution and phase settings for the antennas of the AMC-4 system, as numerically optimised to simulate target heating with the highest T_{90} , with constraints of 44 °C to all tissues.

	Power contribution (%)				Phase (°)			
	Top	Bottom	Left	Right	Top	Bottom	Left	Right
Phantoms^a								
Small homogeneous, central	37.9	37.9	12.1	12.1	0	0	102	102
Small homogeneous, eccentric	49.2	29.9	8.1	12.7	0	-35	-27	-9
Small inhomogeneous, central	28.0	28.0	22.0	22.0	0	0	112	112
Small inhomogeneous, eccentric	49.8	17.8	17.7	14.7	0	-44	-21	-31
Large homogeneous, central	28.2	28.3	21.8	21.7	0	0	56	54
Large homogeneous, eccentric	28.6	28.6	21.4	21.4	0	47	73	74
Large inhomogeneous, central	36.7	36.7	13.3	13.3	0	0	57	57
Large inhomogeneous, eccentric	40.7	29.2	15.1	15.1	0	61	78	78
Patients								
Cervix, small fatless	18.0	4.6	42.8	34.7	0	-67	61	48
Prostate, small fatless	26.8	23.4	27.1	22.7	0	-53	35	1
Bladder, small fatless	17.9	6.1	30.0	45.9	0	-79	26	42
Rectum, small fatless	9.6	12.8	20.0	57.7	0	14	28	71
Cervix, small	14.5	11.9	36.7	36.8	0	-34	109	102
Prostate, small	11.8	33.6	21.1	33.5	0	-18	107	109
Bladder, small	22.8	19.0	12.2	46.0	0	-20	41	47
Rectum, small	3.0	21.5	47.2	28.2	0	119	162	147
Cervix, large	29.2	22.0	24.6	24.2	0	-33	106	101
Prostate, large	19.6	28.2	24.1	28.2	0	-49	59	53
Bladder, large	23.6	30.0	18.9	27.5	0	-20	78	89
Rectum, large	18.2	32.4	22.1	27.4	0	-22	73	94

^aSlight asymmetries in antenna settings could occur for symmetric situations as a result of the Yee-cell used in FDTD calculations [83]. Moreover, optimal settings found are not necessarily unique and other settings might yield similar effective target heating with a different pattern of normal tissue heating.

This can be explained by the higher frequency used in the radiative system, leading to a higher absorption of the electromagnetic field in the superficial layers of the homogeneous phantom, and consequently to a lower

penetration depth into the phantom. Both the central and the eccentric target region are heated effectively, though the predicted temperature in the eccentric target is slightly higher.

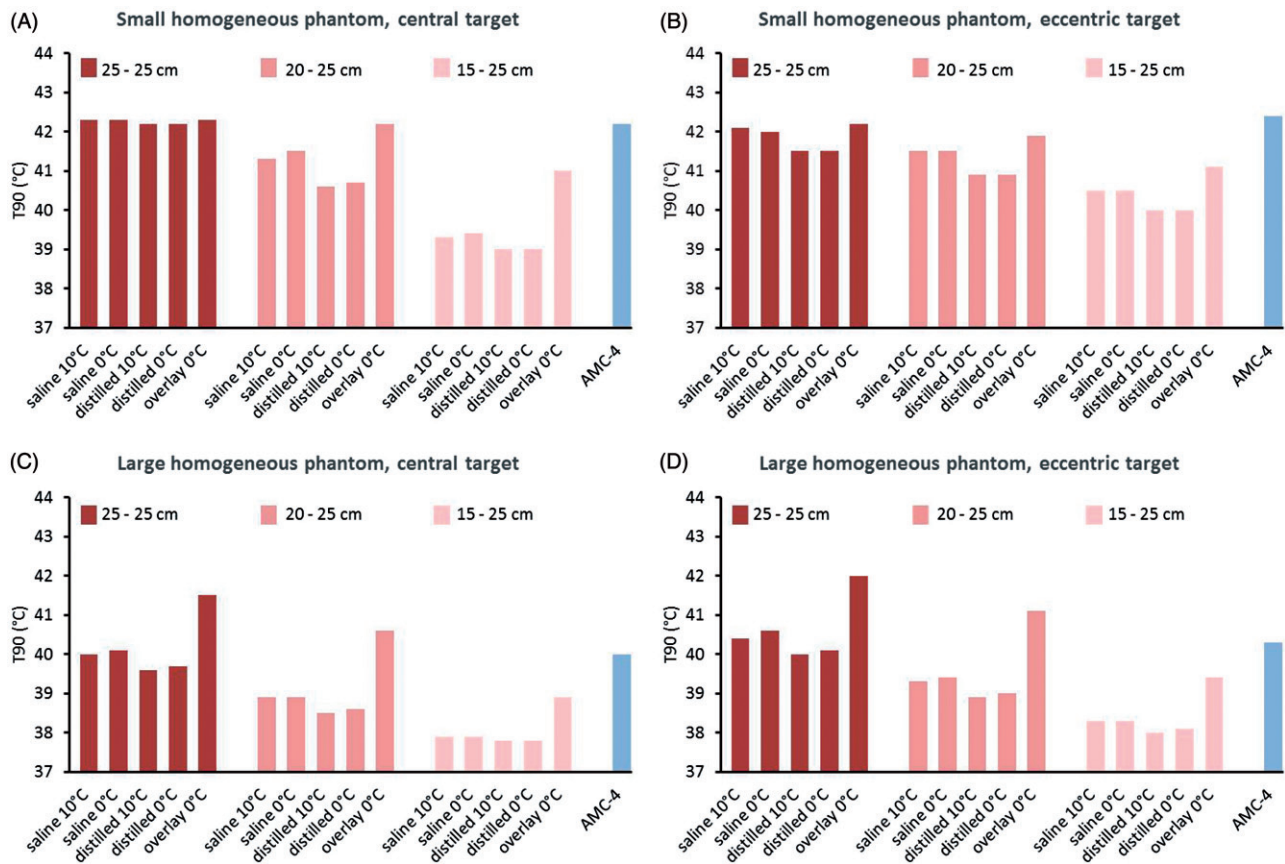


Figure 4. Simulated T_{90} target temperatures for small (A + B) and large (C + D) homogeneous phantoms, with a central or eccentric target volume, heated by different combinations of capacitive electrodes (diameters 25 + 25 cm, 20 + 25 cm or 15 + 25 cm) with different boluses (saline, distilled water, saline + overlay bolus) or the radiative AMC-4 system. Capacitive electrodes were positioned at the top and bottom of the phantom.

Positioning the electrodes at the top and bottom of the phantom is clearly more effective than heating with electrodes positioned at the sides, which can be explained by the smaller distance to the target, similar to heating a smaller phantom. However, heating by electrodes at the sides can be used in combination with heating by electrodes at the top and bottom to lower the average amount of power absorbed in superficial layers of normal tissue. Heating alternately with a short duty cycle through electrodes at the top and bottom or at the sides can improve target heating, especially for the large phantom. Nevertheless, in general the predicted differences with heating using top and bottom electrodes combined with overlay boluses are small.

Figure 4 compares the target T_{90} predicted for different top and bottom electrode combinations, i.e. 25 + 25 cm, 20 + 25 cm and 15 + 25 cm. The combination with two equally sized electrodes yields the highest T_{90} both for the central and eccentric target region. When different sizes of electrodes are combined, the focus of the power absorption is directed towards the smallest electrode. When using different sizes of electrodes for the small phantom with eccentric target, the maximum temperature of 44 °C is still predicted in the target, but the deepest part of the target is less effectively heated compared with equally sized electrodes, which explains the lower T_{90} . For the large phantom, the direction of the power towards the smallest electrode gives rise to hot spots between the bolus of the smallest electrode and the target region and limits effective target heating.

Figure 5 shows the simulated temperature distributions in the central transversal slice for the small and large homogeneous phantoms heated with the AMC-4 system or capacitive electrodes with a saline electrode bolus and overlay bolus. These pictures show that radiative and capacitive heating are equally effective in target heating for the small phantom. However, for the eccentric target location capacitive heating is more target-selective since the maximum normal tissue temperature is ~ 2 °C lower compared with the maximum target temperature of 44 °C, while for radiative heating the maximum normal tissue temperature is also 44 °C. For the large phantom, capacitive heating is more effective and superficial hot spots can be observed with both techniques. The power absorbed in the target region is typically smaller for the large phantom compared to the small one. The same holds for the central target compared to the eccentric target.

Inhomogeneous phantoms

Figure 6 shows the simulated T_{90} for the small and large inhomogeneous fat-muscle phantom, with a central or eccentric target location, heated with the AMC-4 system or capacitive electrodes with a diameter of 25 cm. Figure 7 compares different top and bottom electrode combinations, i.e. 25 + 25 cm, 20 + 25 cm and 15 + 25 cm, and Figure 8 shows the temperature distributions for the inhomogeneous phantoms. Again, outside the target region the maximum temperature is 44 °C for all cases. General aspects about

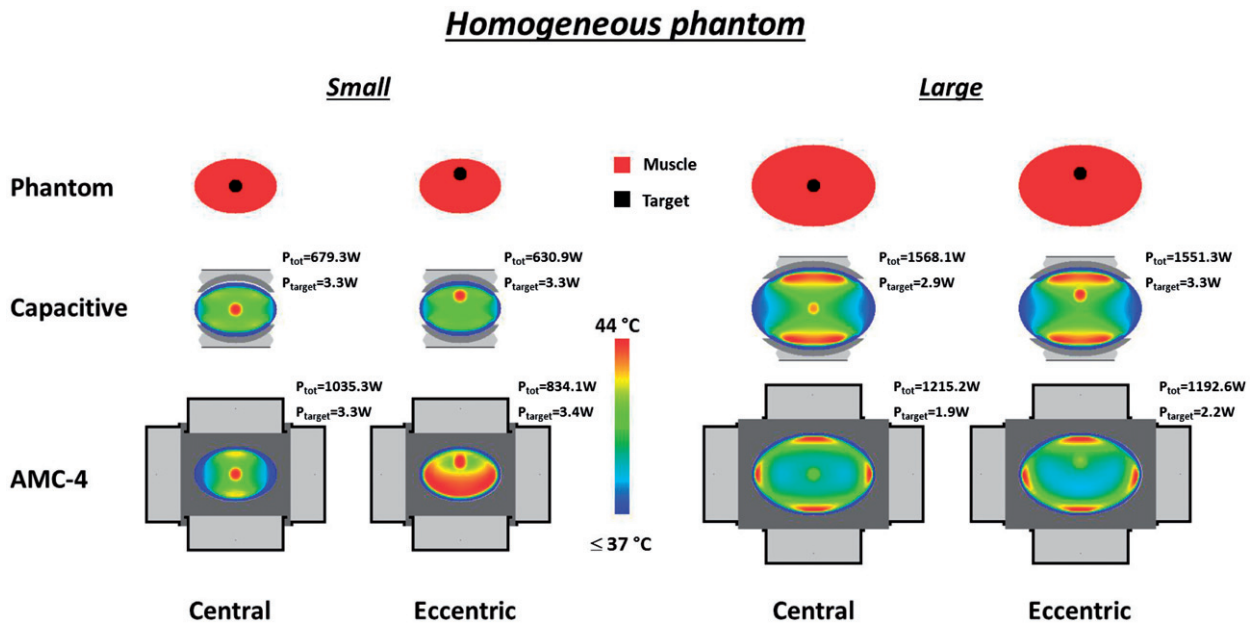


Figure 5. Simulated temperature distributions for heating of the homogeneous phantoms with capacitive electrodes (25 + 25 cm) using overlay boluses and the radiative AMC-4 system. The maximum temperature in all distributions is 44 °C. The total power absorbed in the phantom (P_{tot}) and in the target region (P_{target}) is indicated for each distribution.

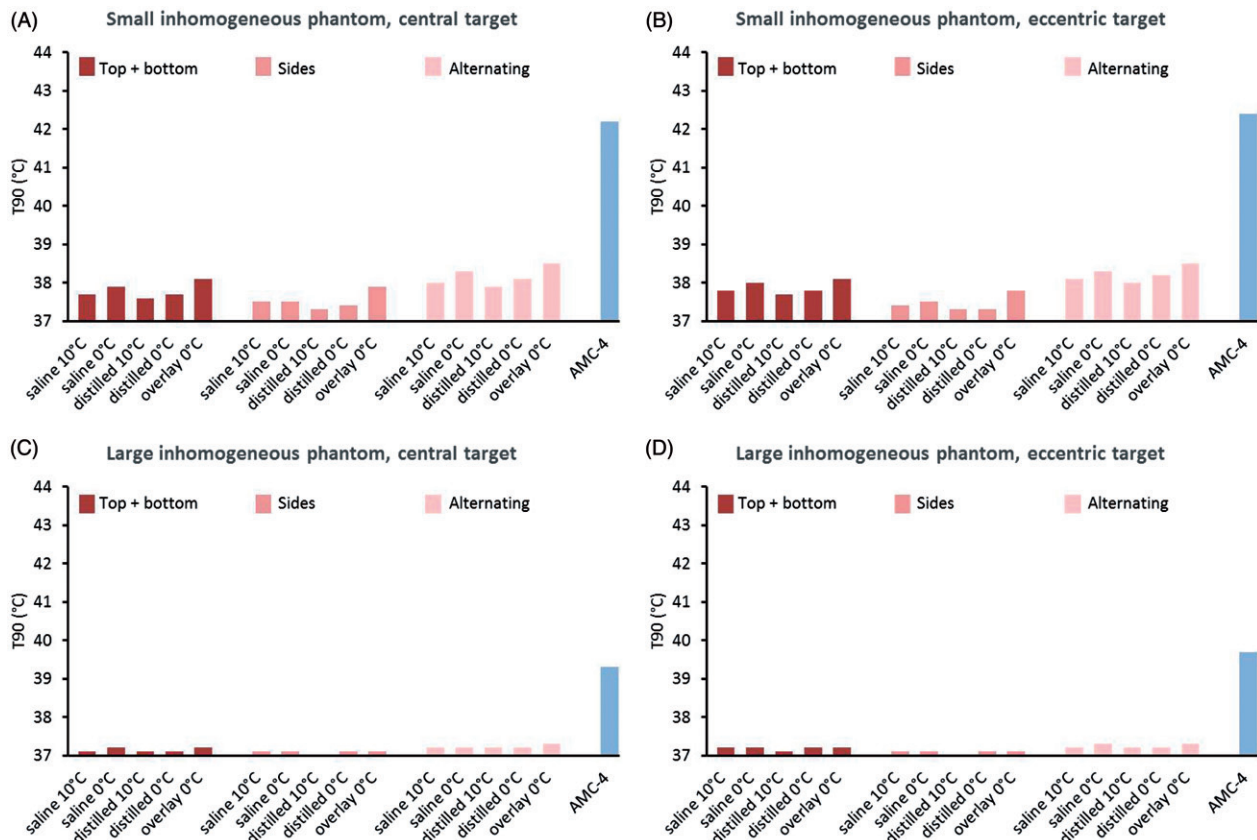


Figure 6. Simulated T_{90} target temperatures for small (A + B) and large (C + D) inhomogeneous phantoms, with a central or eccentric target volume, heated by two 25 cm diameter capacitive electrodes with different boluses (saline, distilled water, saline + overlay bolus) or the radiative AMC-4 system. Capacitive electrodes were positioned at the top and bottom of the phantom, at the sides, or alternatingly.

phantom sizes, bolus filling, water bolus temperature, distance from the antennas or electrodes to the target etc., as mentioned above for the homogeneous phantoms are also valid for the inhomogeneous phantoms. The use of an

overlay bolus still shows the best performance for capacitive heating, but the differences compared with a saline electrode bolus only is now reduced to 0.1–0.2 °C. Target heating for inhomogeneous phantoms is limited by hot spots in normal

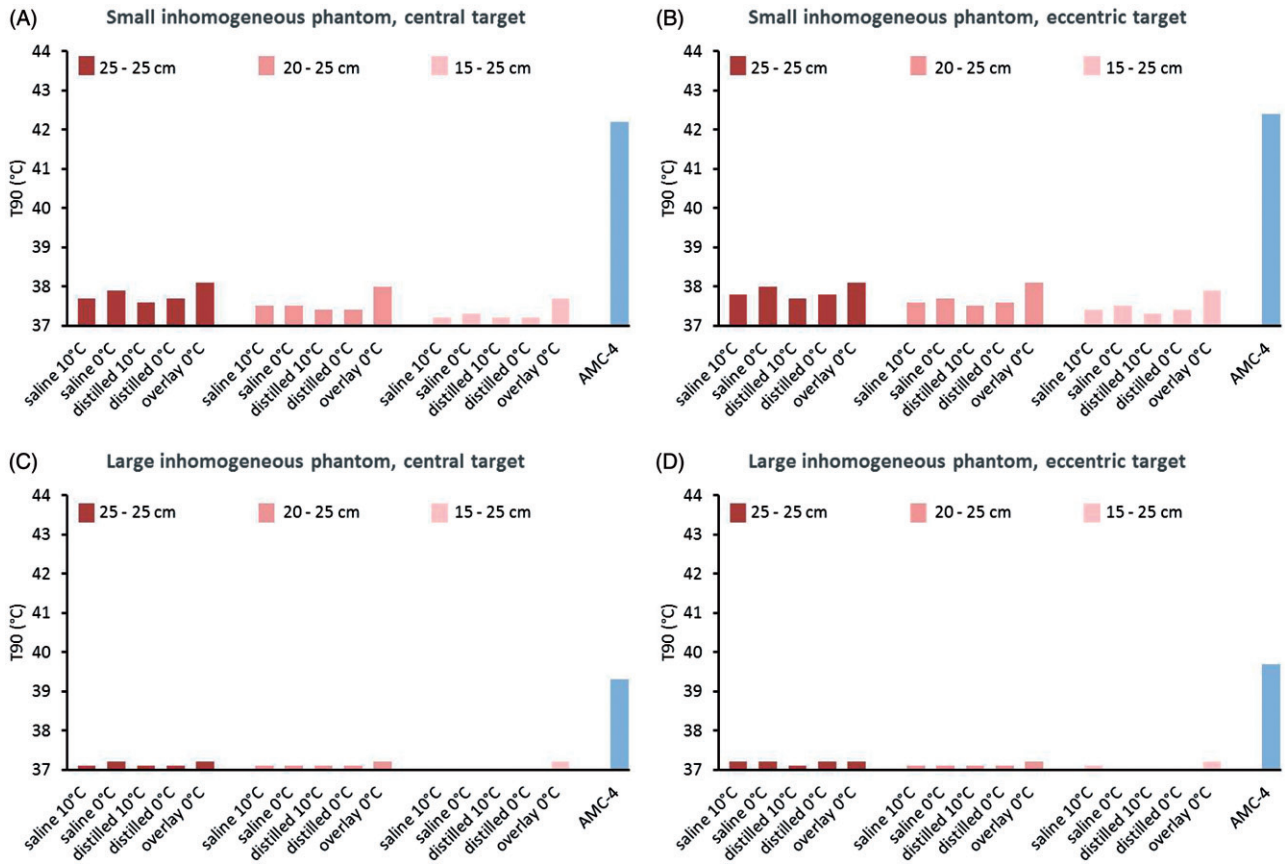


Figure 7. Simulated T_{90} target temperatures for small (A + B) and large (C + D) inhomogeneous phantoms, with a central or eccentric target volume, heated by different combinations of capacitive electrodes (diameters 25 + 25 cm, 20 + 25 cm or 15 + 25 cm) with different boluses (saline, distilled water, saline + overlay bolus) or the radiative AMC-4 system. Capacitive electrodes were positioned at the top and bottom of the phantom.

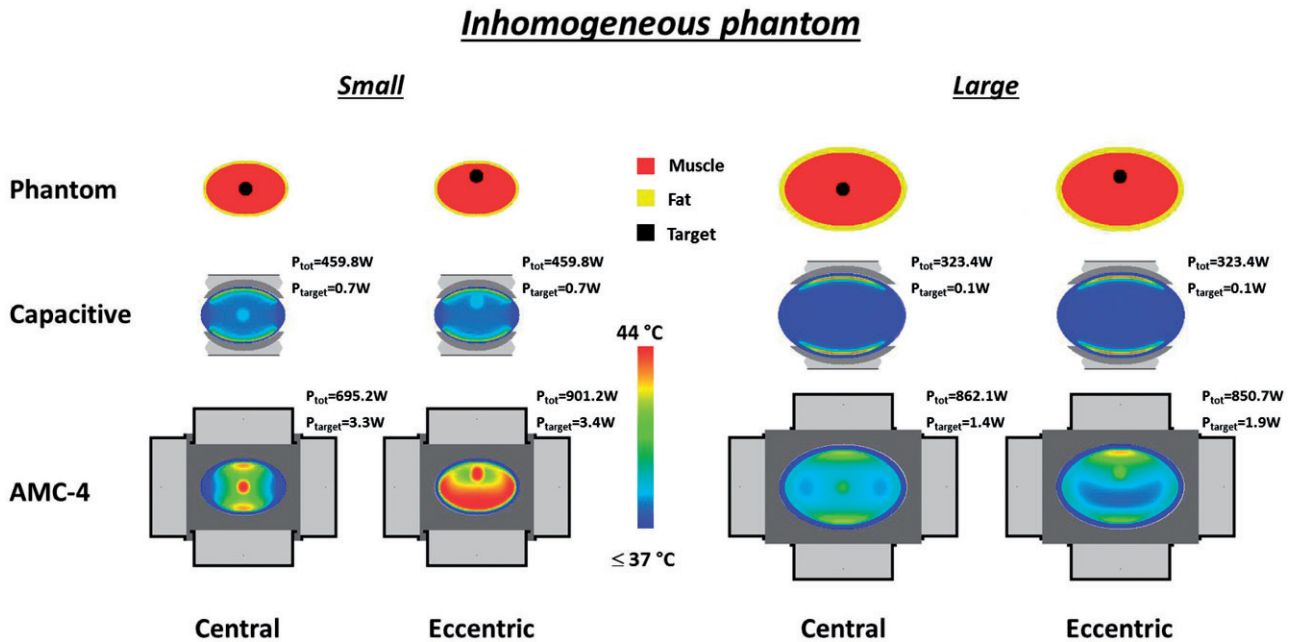


Figure 8. Simulated temperature distributions for heating of the inhomogeneous phantoms with capacitive electrodes (25 + 25 cm) using overlay boluses or the radiative AMC-4 system. The maximum temperature in all distributions is 44°C . The total power absorbed in the phantom (P_{tot}) and in the target region (P_{target}) is indicated for each distribution.

tissue for all cases, both for capacitive and radiative heating. Simulated target temperatures are substantially lower using capacitive electrodes compared with the radiative AMC-4 system, which implies that the hot spots at the fat-muscle

interface are more treatment limiting with capacitive heating compared with radiative heating. Differences in predicted target T_{90} are $\sim 2\text{--}4^{\circ}\text{C}$. The T_{90} predicted with capacitive heating is very low for both the small and the large

inhomogeneous phantom. A target $T_{90} < 37.5^\circ\text{C}$ is observed for the large phantom.

Effect of precooling

Precooling is often applied in the clinic to reduce the incidence of treatment limiting hot spots with capacitive heating. The effect of 15 min precooling with saline water boluses at 10°C was evaluated for the small inhomogeneous phantom with a central target. Figure 9 shows the simulated

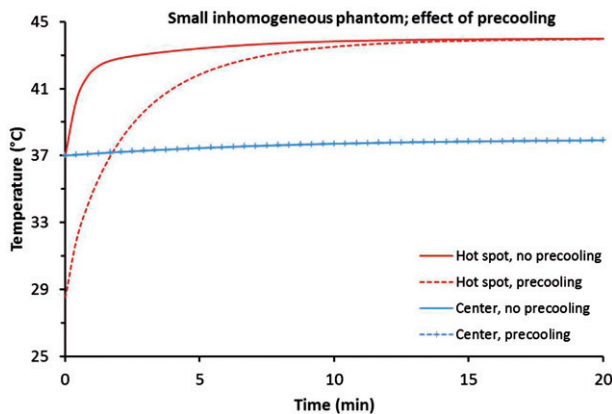


Figure 9. Transient temperature development in the central target region and at a superficial hot spot location at the fat-muscle interface (i.e. at $\sim 1\text{ cm}$ depth) for capacitive heating of the small inhomogeneous phantom with and without 15 min precooling using a saline bolus at 10°C .

transient temperature development with and without precooling for a superficial hot spot location at the fat-muscle interface (i.e. at $\sim 1\text{ cm}$ depth) and the centre of the target region. The temperature development was evaluated at the voxel of the hot spot and at the central voxel of the target region. Precooling affects neither the central target temperature nor the steady-state hot spot temperature. However, when precooling is applied the critical temperature of 44°C at the hot spot location is reached with a delay of a few minutes.

Patient simulations

Figure 10 shows the indexed target temperatures T_{10} , T_{50} and T_{90} for the small fatless, small and large patients with cervix, prostate, bladder and rectum cancer, heated with capacitive electrodes or the radiative AMC-4 system. For capacitive heating, standard top+bottom electrodes were used with saline electrode boluses in combination with overlay boluses, as this showed optimal performance in the phantom simulations. The maximum tissue temperature was 44°C for all cases. Optimized antenna settings for the AMC-4 system are listed in Table 3.

For the small fatless patients, capacitive heating predicts adequate target temperatures for all cases, with simulated T_{90} values above 39.5°C . Heating with the radiative AMC-4 system is predicted to be even more effective, with T_{90}

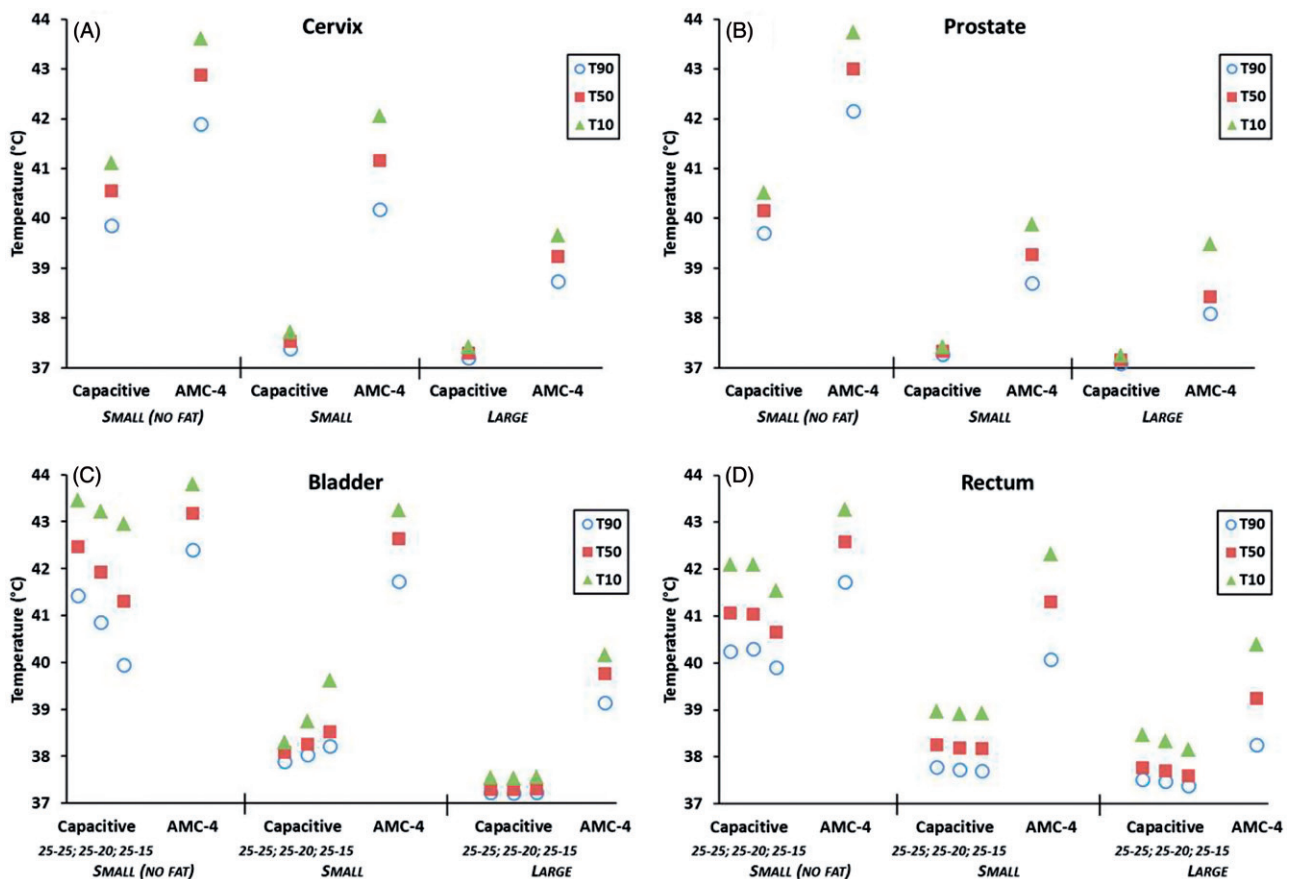


Figure 10. Simulated indexed target temperatures T_{10} , T_{50} and T_{90} , for small fatless, small and large cervix, prostate, bladder and rectum cancer patients heated with capacitive electrodes using overlay boluses with different combinations of capacitive electrodes (diameters $25 + 25\text{ cm}$ for cervix and prostate and diameters $25 + 25\text{ cm}$, $20 + 25\text{ cm}$ or $15 + 25\text{ cm}$ for bladder and rectum) or the radiative AMC-4 system.

values above 41.5°C. However, for the small patients with realistic fat layers the predicted differences in performance are more pronounced. For the centrally located cervix and prostate tumours predicted target temperatures remained between 37 and 38°C for capacitive heating, while with radiative heating a T_{90} of 40.2°C and 38.7°C were simulated for the small patient, respectively. Although mild temperatures of about ~39°C are considered sub-optimal, still some relevant positive biological effects on enhancement of radiotherapy (e.g. re-oxygenation by increased blood flow) are expected [54]. However, in view of the clinically established thermal dose-effect relationship treatment outcome is likely to improve with increasing target temperatures [3,5,9].

For the more eccentrically located bladder and rectum tumours, capacitive heating was predicted to perform better than for the centrally located tumours. Different sizes of electrodes are clinically used to focus heating towards eccentric locations. However, the anatomy and the exact location of the target determine whether different sizes of electrodes improve target heating compared with equally sized electrodes. Figure 10(C) shows that for the small fatless bladder cancer patient results are in correspondence with the phantom simulations and equally sized electrodes yield the best predicted temperatures, while for the small bladder patient a smaller top electrode indeed improves target coverage. For the small patient, the simulated T_{90} increased from 37.9°C to 38.2°C when a top electrode with a diameter of 15 cm instead of 25 cm was used. For the

rectum tumour (Figure 10(D)), which is more deep-seated than the bladder tumour, this had no effect and the T_{90} for the small rectum cancer patient was 37.7°C. Since the simulated T_{50} and T_{10} were also below 39°C, such a treatment would not be expected to be very effective [54]. For these eccentric tumours, radiative heating was again much more effective: the T_{90} simulated with the AMC-4 system was 41.7°C and 40.1°C for the small bladder and rectum cancer patients, respectively. These simulated temperatures are in the therapeutic range and thus can be expected to yield an effective treatment [54]. Figure 11 shows that a 10% increase in conductivity of the tumour target region, an increase sometimes found in the literature [49,50], has a negligible effect on simulated tumour temperature levels.

In general, large patients are more difficult to heat and as for the phantom simulations, again a better target heating was simulated for the smaller patients, both with capacitive and radiative heating. However, in large patients almost no target heating was predicted with capacitive heating without overheating normal tissue, while for radiative heating still T_{90} temperatures above 38°C were predicted and T_{50} was above 39°C in most cases.

Figures 12 and 13 show transversal and sagittal slices of the simulated temperature distributions for the small fatless cervix, prostate, bladder and rectum patients. These distributions demonstrate that capacitive heating could realise therapeutic heating when (superficial) fat layers are absent. Nevertheless, even in those cases a more pronounced

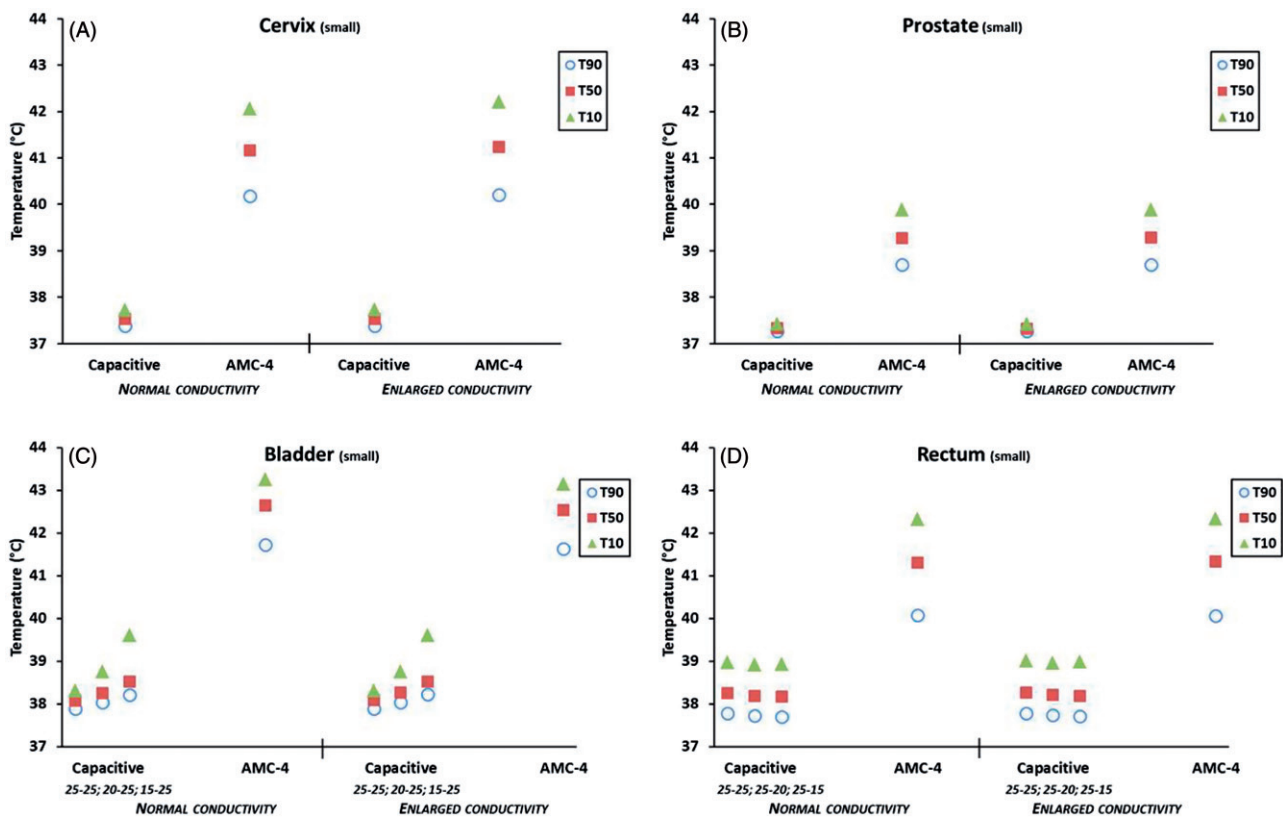


Figure 11. Simulated indexed target temperatures T_{10} , T_{50} and T_{90} for small cervix, prostate, bladder and rectum cancer patients with normal electrical conductivity of the target region, or 10% enlarged values of the electrical conductivity. Heating was simulated with capacitive electrodes using overlay boluses with different combinations of capacitive electrodes (diameters 25 + 25 cm for cervix and prostate and diameters 25 + 25 cm, 20 + 25 cm or 15 + 25 cm for bladder and rectum) or the radiative AMC-4 system.

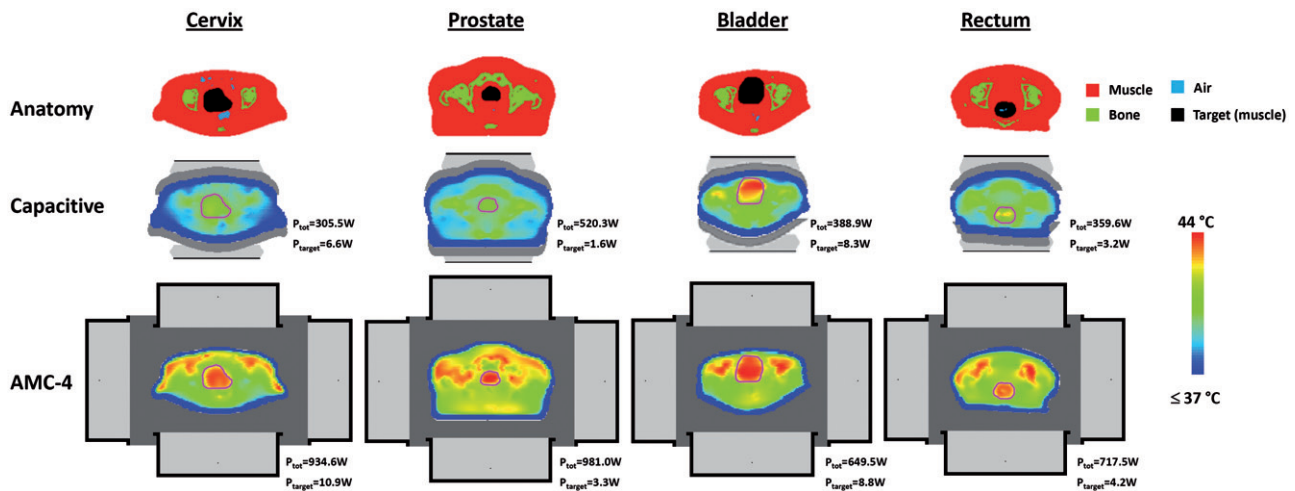


Figure 12. Transversal slices of the simulated temperature distribution for small fatless cervix, prostate, bladder and rectum cancer patients heated with capacitive electrodes (25 + 25 cm) using overlay boluses or the radiative AMC-4 system. The maximum temperature in all distributions is 44 °C. The total power absorbed in the patient (P_{tot}) and in the target region (P_{target}) is indicated for each distribution. Cross-sections are at the centre of the target region in axial direction. The contour in the temperature distributions indicates the target region.

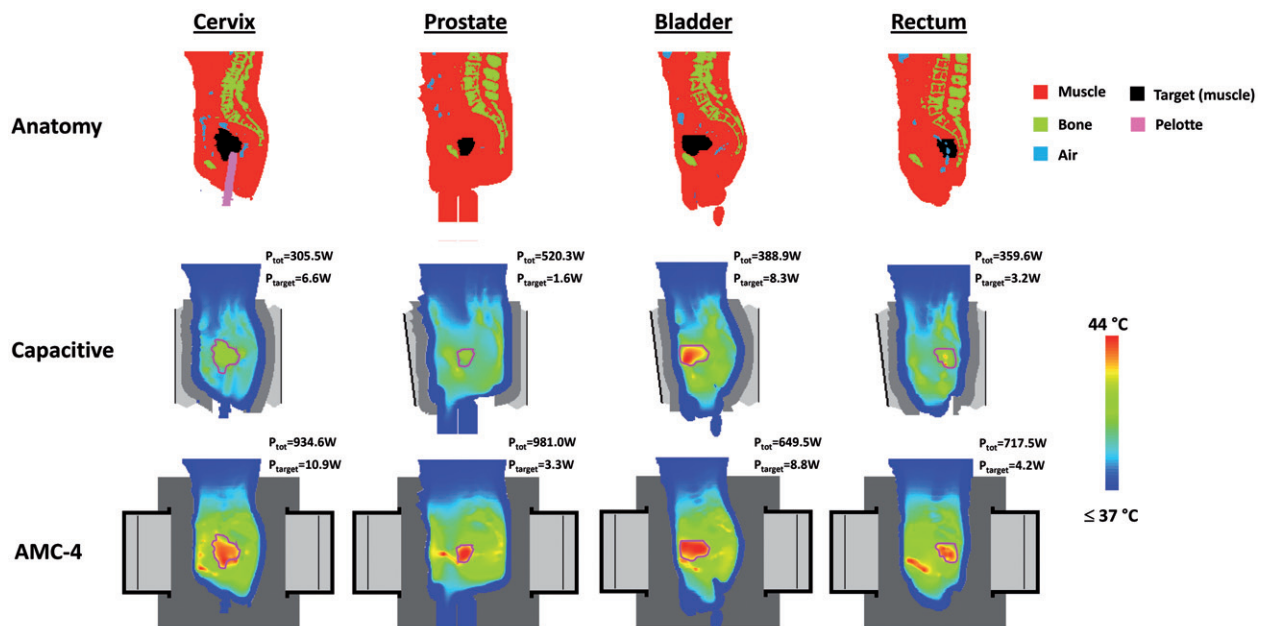


Figure 13. Sagittal slices of the simulated temperature distribution for small fatless cervix, prostate, bladder and rectum cancer patients heated with capacitive electrodes (25 + 25 cm) using overlay boluses or the radiative AMC-4 system. The maximum temperature in all distributions is 44 °C. The total power absorbed in the patient (P_{tot}) and in the target region (P_{target}) is indicated for each distribution. Slices were taken approximately through the centre of the patient. The contour in the temperature distributions indicates the target region.

heating focus is predicted for heating with the radiative AMC-4 system. Figures 14 and 15 show the simulated distributions for the small patients. These figures demonstrate the limited deep-seated heating using capacitive electrodes due to the incidence of superficial hot spots, despite the aggressive skin cooling. With radiative heating, hot spots are less treatment limiting and higher temperatures are predicted at deep-seated locations, although a pronounced heating focus in the target region is not observed due to treatment limiting hot spots (with exception of the bladder). This is also reflected in the total power absorbed in the patient and in the target region, which is substantially larger for radiative heating.

Discussion

In this study, a comparison of temperature distributions in perfused small and large muscle tissue and fat-muscle phantoms as well as small and large cervix, prostate, bladder and rectum cancer patients showed that radiative hyperthermia is generally more effective in heating deep-seated pelvic tumour locations than capacitive hyperthermia. Substantially higher target temperatures (1–3 °C higher T_{90}) were predicted with radiative heating before treatment limiting hot spots in normal tissues occurred. These results confirm and extend observations of Kroeze *et al.*, who demonstrated for a single prostate cancer patient that adequate tumour

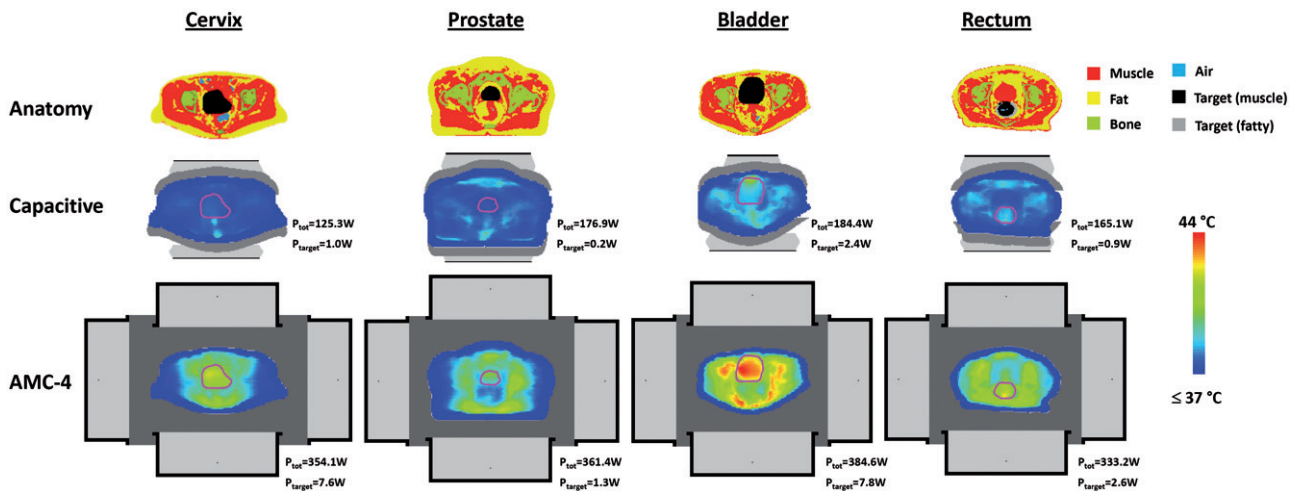


Figure 14. Transversal slices of the simulated temperature distribution for small cervix, prostate, bladder and rectum cancer patients heated with capacitive electrodes using overlay boluses or the radiative AMC-4 system. Electrode sizes top + bottom were 25 + 25 cm (cervix, prostate, rectum) and 15 + 25 cm (bladder). The maximum temperature in all distributions is 44 °C. The total power absorbed in the patient (P_{tot}) and in the target region (P_{target}) is indicated for each distribution. Cross-sections are at the centre of the target region in axial direction. The contour in the temperature distributions indicates the target region.

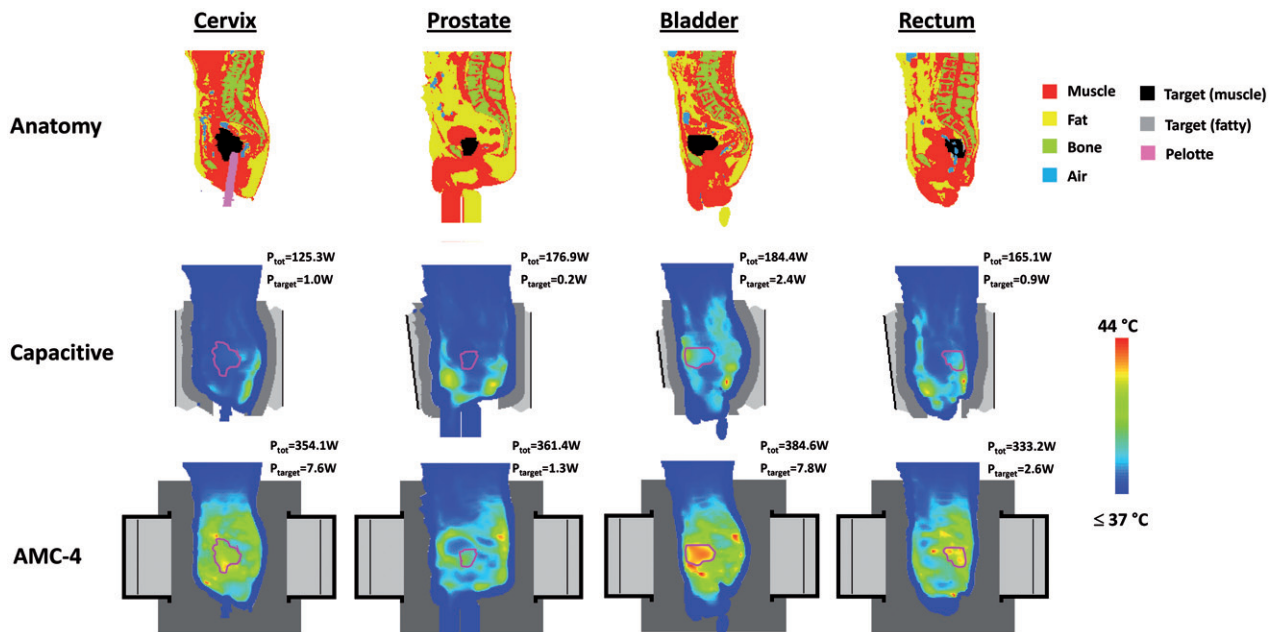


Figure 15. Sagittal slices of the simulated temperature distribution for small cervix, prostate, bladder and rectum cancer patients heated with capacitive electrodes using overlay boluses or the radiative AMC-4 system. Electrode sizes top + bottom were 25 + 25 cm (cervix, prostate, rectum) and 15 + 25 cm (bladder). The maximum temperature in all distributions is 44 °C. The total power absorbed in the patient (P_{tot}) and in the target region (P_{target}) is indicated for each distribution. Slices were taken approximately through the centre of the patient. The contour in the temperature distributions indicates the target region.

temperatures can only be obtained with capacitive heating when accepting very high temperatures in the superficial fat and muscle layers [30,32].

Results of the present study showed that large patients with deep-seated tumours are more difficult to heat than small patients, both for capacitive and radiative heating. This can be explained by the larger distance of the electrode/antenna to the target location. This phenomenon is also observed in the clinic, as described by Van Haaren *et al.*, who demonstrated that intra-oesophageal temperatures during locoregional hyperthermia are inversely related to patients' body size parameters, of which fat percentage is the most significant prognostic factor [55]. Hiraoka *et al.* also observed

that the heating efficacy decreased with increasing fat thickness in a study with a diverse patient population consisting of deep-seated malignancies in the upper abdomen, lower abdomen, pelvis, thorax, the head and neck and lower extremities [12].

We simulated a number of strategies to improve the effectiveness of capacitive heating. The water bolus filling has some influence on the predicted temperature distribution with capacitive heating and the use of a saline electrode bolus combined with an overlay bolus as proposed by Kato [16], provides very aggressive cooling of the skin such that higher tumour temperatures could be achieved compared with saline or distilled water filled electrode boluses only.

Precooling is often applied clinically in order to reduce the incidence of treatment limiting hot spots with capacitive heating [56], even though clinical experience shows that this is not always effective in avoiding preferential heating at fat–muscle interfaces [57]. Simulations showed that despite the precooling the same steady state temperature is predicted, both at the superficial hot spot and at the target location. Precooling in combination with switching the active electrodes from top and bottom to the sides can improve patient comfort since hot spot complaints are resolved temporarily. However, the target temperature is not expected to improve sufficiently to realise a substantial improvement in treatment outcome. The simulations performed in this study for alternatingly heating with electrodes at the top and bottom and at the sides assumed a continuous switching with a very short duty cycle (e.g. 30 s) and continuous overall skin cooling to model the optimal result that can theoretically be achieved with this switching technique. However, steady state temperatures were very similar to those predicted with electrodes at the top and bottom using saline electrode boluses in combination with overlay boluses. The fundamental problem that causes the treatment limiting hot spots is the E-field direction that is perpendicular to the fat–muscle interface in combination with the lack of steering possibilities. Switching electrode positions does not overcome these fundamental problems, but continuously changes the location of the treatment limiting hot spot which does improve the target temperature, but again not sufficiently to meet the clinical requirements. Moreover, switching active electrode positions makes the treatment more complicated and it is only feasible with more flexible capacitive heating systems.

The differences in behaviour between capacitive and radiative heating can be explained by evaluating the electromagnetic field emitted by the two systems. The capacitive electrodes produce an electric field (E-field) that is oriented mainly perpendicular to the superficial fat–muscle interfaces, while for the radiative antennas the main E-field direction is parallel to the superficial fat–muscle interfaces. The interface conditions derived from Maxwell's equations prescribe that the tangential E-field is continuous, while the normal E-field component undergoes a discontinuity proportional to the dielectric properties of the two different tissues. This yields a much higher value of the electric field in the fat tissue for the capacitive systems, which explains the treatment limiting hot spots. Moreover, the possibility to focus the electromagnetic field is very minimal with capacitive heating, since only different electrode sizes can be chosen. Radiative heating is typically performed with phased-array systems providing phase-amplitude steering to focus heating to the target and minimise hot spots. This explains that treatment limiting hot spots at fat-muscle tissue interfaces are more dominant for capacitive heating than for radiative heating and that adaptations in bolus cooling etc. to improve capacitive heating only have a limited effect.

Capacitive and radiative heating were compared using treatment planning to demonstrate qualitative differences between heating effectiveness. Treatment planning has been successfully applied for similar applications comparing

different heating techniques, frequencies and antenna designs [18,20,26,58–60]. Planning is very reliable for application in phantoms with known material properties. However, quantitative results are less reliable in clinical application due to the uncertainties in exact tissue properties and perfusion, so the results can only be translated qualitatively to clinical settings, both for capacitive and radiative heating. For some cases hardly any temperature rise was predicted in the target region for capacitive heating, and in reality for these cases the target temperature might be increased for example with 1–2 °C, since a clinical study by Ohguri *et al.* reports a median T_{90} between 38 °C and 39 °C for cervical cancer patients [3]. A temperature-dependent perfusion model could improve the reliability of the thermal simulations [61–63], but requires very long computation times and uncertainties in the exact perfusion values will still remain. We chose to use perfusion values which are representative when tissues are subjected to hyperthermic temperature levels, but higher than the perfusion values expected at temperatures <38 °C. This will lead to a slight underestimation of the lowest predicted temperature increase. All normal tissue constraints were set to 44 °C, while some studies report that patients can tolerate fat temperatures of 45 °C before complaining [57], which would imply that all target temperatures could increase with roughly 15%, both for radiative and capacitive heating. However, since important model parameters in this study, such as tissue properties, perfusion values and temperature constraints, were the same for both capacitive and radiative heating, the qualitative differences in predicted temperatures between capacitive and radiative heating will remain valid, despite the uncertainties in (thermal) modelling. Clinical treatment planning has proven to be effective in predicting qualitative differences in heating quality. For example, Sreenivasa *et al.* reported that treatment planning can predict whether patients are easy-to-heat or difficult-to-heat [64], and Kok *et al.* demonstrated that treatment planning is effective to predict relative differences in heating patterns [65–67].

For radiative heating, the 2D 70 MHz AMC-4 phased array system was modelled in this study. Other radiative locoregional heating systems are commercially available, such as the 75–120 MHz BSD-2000 Sigma-60 system [21], the 100 MHz BSD-2000 Sigma-Eye system [19] and the 70 MHz ALBA 4D system [68]. Such phased array systems all provide phase-amplitude steering to focus the electromagnetic energy and avoid hot spots [69]. Some of these systems provide 3D steering to realise a more favourable power and temperature distribution compared with 2D steering. Therefore, the qualitative differences in heating quality in favour of radiative heating as demonstrated in this paper will be generally valid for 2D radiative heating systems and can be even slightly larger for 3D systems.

Although this study showed that capacitive heating is in general much less effective compared with radiative heating for deep-seated pelvic tumours, capacitive heating can be of clinical value for some specific patient categories. The phantom and patient simulations in this paper showed very effective target heating when no fat layer is present. This was also demonstrated in a recent phantom study by

Sahinbas *et al.* [70], who performed measurements in an agar phantom as well as in the Alderson radiotherapy phantom, which represents soft tissue, lung tissue and bone. These results show that for very slender patients with almost no fat, capacitive heating can be effective for deep-seated tumours. This is confirmed by several positive clinical studies using capacitive heating. For example, Hiraoka *et al.* reported temperatures $>41^{\circ}\text{C}$ in clinical applications [11], and Harima *et al.* reported an increase in 3-year overall survival for stage IIIB cervical carcinoma from 48.1% with radiation alone to 58.2% with radiation plus capacitive heating [71]. Clinical results of Ohguri *et al.* for Japanese cervical cancer patients, showed that the 26 out of 47 patients with a CEM43T90 > 1 showed a significantly better clinical outcome than the remaining 21 patients who proved impossible to heat with a CEM43T90 < 1 [3]. Pancreatic cancer patients tend to be more slender than other categories, so fat may be nearly absent in pancreatic cancer patients and clinical temperature data reported from small patients series indicate that therapeutic temperatures exceeding 42°C are achievable for this patient category using capacitive devices [72–74].

Our predictions suggest that eccentrically located tumours (i.e. rectum and bladder) do relatively better for capacitive heating compared with centrally located tumours (i.e. cervix and prostate). Accordingly, another patient category for which capacitive heating might be considered is large eccentrically located bulky tumours, such as breast tumours or head and neck tumours. Clinical studies report feasibility of heating bulky tumours with capacitive systems with tumour temperatures in the therapeutic range ($40\text{--}44^{\circ}\text{C}$) [17,75–77]. Some caution is required though, since clinically measured temperatures using a limited number of thermometry probes do not provide full information about the 3D temperature distribution and extensive thermometry would be necessary to avoid missing hot spots that could lead to subcutaneous burns [57]. Van Wieringen *et al.* described clinical application of capacitive heating with a 70 MHz CFMA for 6 patients with bulky breast tumours and concluded that the penetration depth is adequate and acceptable temperatures were realised, but temperature distributions were very heterogeneous and hot spots were often treatment limiting [78]. A study by Kok *et al.* compared radiative and capacitive heating with a 70 MHz CFMA for a bulky tumour on the leg, and retrospective treatment planning results corresponded qualitatively to temperatures measured during clinical treatments [28,29]. This study showed that with radiative heating a better tumour coverage was achieved. Again, with capacitive heating treatment limiting hot spots were more dominant. Although the dominant E-field component is not perpendicular but parallel to the fat-muscle interface for the capacitive 70 MHz CFMA, the perpendicular E-field component is still relatively high, which explains the treatment limiting hot spots [78]. Thus, in general a better tumour coverage is expected when using radiative heating, also for bulky tumours.

For superficial tumours infiltrating up to 4 cm into tissue, such as chest wall recurrences, capacitive heating can be effective since the use of a significantly smaller electrode on the tumour can effectively steer the power towards the

surface. Therapeutic temperatures can indeed be realised as demonstrated in a previous simulation study [27]. However, also in this study radiative heating performed substantially better as T_{90} was $0.4\text{--}1.1^{\circ}\text{C}$ higher than with capacitive heating.

Thus, therapeutic temperatures can be achieved with capacitive heating for some patient categories, but clinical studies have shown that tumour control is correlated to the target temperatures, and especially the minimum temperature is predictive for clinical outcome [53,79–81]. For temperatures below 42.5°C , as usually reported during clinical hyperthermia, an increase of 0.5°C already yields a doubling of the thermal dose, i.e. the cumulative equivalent minutes at 43°C (CEM43) [82]. This makes it important to aim for the highest possible tumour temperature and carefully select the heating equipment for specific patient categories. Treatment planning can be helpful to qualitatively compare the heating effectiveness in order to make a well-considered decision on heating equipment.

Conclusion

This simulation study showed that therapeutic temperatures are predicted for capacitive heating in patients with (almost) no fat. Nevertheless, radiative hyperthermia generally yields much more favourable heating patterns for deep-seated pelvic tumours, compared with capacitive heating. With radiative heating higher tumour temperatures are predicted before treatment limiting hot spots occur, which will benefit clinical outcome.

Disclosure statement

No potential conflict of interest was reported by the authors.

ORCID

M. Cavagnaro  <http://orcid.org/0000-0002-7624-1113>

J. Crezee  <http://orcid.org/0000-0002-7474-0533>

References

- [1] Cihoric N, Tsikkinis A, van Rhoon G, et al. (2015). Hyperthermia-related clinical trials on cancer treatment within the ClinicalTrials.gov registry. *Int J Hyperthermia* 31:609–14.
- [2] Van der Zee J, González González D, Van Rhoon GC, et al. (2000). Comparison of radiotherapy alone with radiotherapy plus hyperthermia in locally advanced pelvic tumours: a prospective, randomised, multicentre trial. Dutch Deep Hyperthermia Group. *Lancet* 355:1119–25.
- [3] Ohguri T, Harima Y, Imada H, et al. (2017). Relationships between thermal dose parameters and the efficacy of definitive chemoradiotherapy plus regional hyperthermia in the treatment of locally advanced cervical cancer: data from a multicentre randomised clinical trial. *Int J Hyperthermia*. [Epub ahead of print]. DOI:10.1080/02656736.2017.1352105
- [4] Maluta S, Dall'oglio S, Romano M, et al. (2007). Conformal radiotherapy plus local hyperthermia in patients affected by locally advanced high risk prostate cancer: preliminary results of a prospective phase II study. *Int J Hyperthermia* 23:451–6.

- [5] Wust P, Rau B, Gellerman J, et al. (1998). Radiochemotherapy and hyperthermia in the treatment of rectal cancer. *Recent Results Cancer Res* 146:175–91.
- [6] Inman BA, Stauffer PR, Craciunescu OA, et al. (2014). A pilot clinical trial of intravesical mitomycin-C and external deep pelvic hyperthermia for non-muscle-invasive bladder cancer. *Int J Hyperthermia* 30:171–5.
- [7] Geijsen ED, De Reijke TM, Koning CCE, et al. (2015). Combining mitomycin C and regional 70 MHz hyperthermia in patients with nonmuscle invasive bladder cancer: a pilot study. *J Urol* 194:1202–8.
- [8] Datta NR, Rogers S, Klingbiel D, et al. (2016). Hyperthermia and radiotherapy with or without chemotherapy in locally advanced cervical cancer: a systematic review with conventional and network meta-analyses. *Int J Hyperthermia* 32:809–21.
- [9] Franckena M, Fatehi D, de Bruijne M, et al. (2009). Hyperthermia dose-effect relationship in 420 patients with cervical cancer treated with combined radiotherapy and hyperthermia. *Eur J Cancer* 45:1969–78.
- [10] Sapareto SA, Dewey WC. (1984). Thermal dose determination in cancer therapy. *Int J Radiat Oncol Biol Phys* 10:787–800.
- [11] Hiraoka M, Jo S, Akuta K, et al. (1987). Radiofrequency capacitive hyperthermia for deep-seated tumors. II. Effects of thermoradiotherapy. *Cancer* 60:128–35.
- [12] Hiraoka M, Jo S, Akuta K, et al. (1987). Radiofrequency capacitive hyperthermia for deep-seated tumors. I. Studies on thermometry. *Cancer* 60:121–7.
- [13] Harima Y, Ohguri T, Imada H, et al. (2016). A multicentre randomised clinical trial of chemoradiotherapy plus hyperthermia versus chemoradiotherapy alone in patients with locally advanced cervical cancer. *Int J Hyperthermia* 32:801–8.
- [14] Tomura K, Ohguri T, Mulder HT, et al. (2017). The usefulness of mobile insulator sheets for the optimization of deep heating area for regional hyperthermia using a capacitively-coupled heating method: phantom, simulation and clinical prospective studies. *Int J Hyperthermia*. [Epub ahead of print]. DOI:[10.1080/02656736.2017.1402130](https://doi.org/10.1080/02656736.2017.1402130)
- [15] Issels RD, Lindner LH, Verweij J, et al. (2010). Neo-adjuvant chemotherapy alone or with regional hyperthermia for localised high-risk soft-tissue sarcoma: a randomised phase 3 multicentre study. *Lancet Oncol* 11:561–70.
- [16] Kato H, Hyodo K, Akassa N, et al. (1997). Optimization of bolus for capacitive type heating. *Jpn J Hyperthermic Oncol* 13:10–7.
- [17] Abe M, Hiraoka M, Takahashi M, et al. (1986). Multi-institutional studies on hyperthermia using an 8-MHz radiofrequency capacitive heating device (Thermotron RF-8) in combination with radiation for cancer therapy. *Cancer* 58:1589–95.
- [18] Paulsen KD, Geimer S, Tang J, et al. (1999). Optimization of pelvic heating rate distributions with electromagnetic phased arrays. *Int J Hyperthermia* 15:157–86.
- [19] Wust P, Seebass M, Nadobny J, et al. (1996). Simulation studies promote technological development of radiofrequency phased array hyperthermia. *Int J Hyperthermia* 12:477–94.
- [20] Kok HP, De Greef M, Borsboom PP, et al. (2011). Improved power steering with double and triple ring waveguide systems: the impact of the operating frequency. *Int J Hyperthermia* 27:224–39.
- [21] Turner PF, Tumeh A, Schaefermeyer T. (1989). BSD-2000 approach for deep local and regional hyperthermia: physics and technology. *Strahlenther Onkol* 165:738–41.
- [22] van Dijk JDP, Schneider CJ, van Os RM, et al. (1990). Results of deep body hyperthermia with large waveguide radiators. *Adv Exp Med Biol* 267:315–19.
- [23] Oleson JR, Sim DA, Conrad J, et al. (1986). Results of a phase I regional hyperthermia device evaluation: microwave annular array versus radiofrequency induction coil. *Int J Hyperthermia* 2:327–36.
- [24] Oleson JR. (1984). Regional power deposition for hyperthermia: theoretical approaches and considerations. *Cancer Res* 44:4761s–4s.
- [25] Kok HP, Wust P, Stauffer PR, et al. (2015). Current state of the art of regional hyperthermia treatment planning: a review. *Radiat Oncol* 10:196.
- [26] Kok HP, De Greef M, Wiersma J, et al. (2010). The impact of the waveguide aperture size of the 3D 70MHz AMC-8 loco-regional hyperthermia system on tumour coverage. *Phys Med Biol* 55:4899–916.
- [27] Kok HP, Crezee J. (2017). A comparison of the heating characteristics of capacitive and radiative superficial hyperthermia. *Int J Hyperthermia* 33:378–86.
- [28] Kok HP, De Greef M, Van Wieringen N, et al. (2010). Comparison of two different 70 MHz applicators for large extremity lesions: simulation and application. *Int J Hyperthermia* 26:376–88.
- [29] Kok HP. (2010). Comparison of two different 70 MHz applicators for large extremity lesions: simulation and application (vol 26, pg 376, 2010). *Int J Hyperthermia* 26:413–14.
- [30] Kroeze H, Kokubo M, van de Kamer JB, et al. (2002). Comparison of a capacitive and a cavity slot radiative applicator for regional hyperthermia. *Jpn J Hyperthermic Oncol* 18:75–91.
- [31] Kok HP, Kotte ANTJ, Crezee J. (2017). Planning, optimisation and evaluation of hyperthermia treatments. *Int J Hyperthermia* 33:593–607.
- [32] Kroeze H, van de Kamer JB, de Leeuw AA, et al. (2003). Treatment planning for capacitive regional hyperthermia. *Int J Hyperthermia* 19:58–73.
- [33] De Bree J. (1998). A 3-D anatomy based treatment planning system for interstitial hyperthermia. PhD Thesis; Utrecht University.
- [34] Crezee J, Van Haaren PMA, Westendorp H, et al. (2009). Improving locoregional hyperthermia delivery using the 3-D controlled AMC-8 phased array hyperthermia system: a preclinical study. *Int J Hyperthermia* 25:581–92.
- [35] Oncotherm. (2017). <http://www.oncotherm.com/>.
- [36] Celsius42+. (2017). <http://www.celsius42.de/>.
- [37] Synchrotherm. (2017). www.synchrotherm.com.
- [38] HY-DEEP 600WM. (2017). <http://www.andromedic.it/>.
- [39] Thermotron RF-8. (2017). <http://www.mpr-cro.com/thermotron/>.
- [40] Ohguri T, Imada H, Yahara K, et al. (2004). Effect of 8-MHz radiofrequency-capacitive regional hyperthermia with strong superficial cooling for unresectable or recurrent colorectal cancer. *Int J Hyperthermia* 20:465–75.
- [41] Ohguri T, Imada H, Kato F, et al. (2006). Radiotherapy with 8 MHz radiofrequency-capacitive regional hyperthermia for pain relief of unresectable and recurrent colorectal cancer. *Int J Hyperthermia* 22:1–14.
- [42] Hornsleth SN, Mella O, Dahl O. (1996). A new segmentation algorithm for finite difference based treatment planning systems. In: Franconi C, Arcangeli G, Cavaliere R, eds. *Hyperthermic oncology*, vol. 2. Rome, Italy: Tor Vergata, 521–523.
- [43] Taflove A, Hagness SC. (2000). *Computational electrodynamics*. 2nd ed. Boston, London: Artech House.
- [44] Berenger JP. (1994). A perfectly matched layer for the absorption of electromagnetic-waves. *J Comput Phys* 114:185–200.
- [45] de Bree J, van der Koijk JF, Lagendijk JJW. (1996). A 3-D SAR model for current source interstitial hyperthermia. *IEEE Trans Biomed Eng* 43:1038–45.
- [46] Gabriel S, Lau RW, Gabriel C. (1996). The dielectric properties of biological tissues: II. Measurements in the frequency range 10 Hz to 20 GHz. *Phys Med Biol* 41:2251–69.
- [47] ESHO Taskgroup Committee, "Treatment Planning and Modelling in Hyperthermia, a Task Group Report of the European Society for Hyperthermic Oncology (Rome, Italy: Tor Vergata)," 1992.
- [48] Rossmann C, Haemmerich D. (2014). Review of temperature dependence of thermal properties, dielectric properties, and perfusion of biological tissues at hyperthermic and ablation temperatures. *Crit Rev Biomed Eng* 42:467–92.
- [49] Balidemaj E, de Boer P, van Lier AL, et al. (2016). In vivo electric conductivity of cervical cancer patients based on B(1)(+) maps at 3T MRI. *Phys Med Biol* 61:1596–607.

- [50] Raouf M, Cisneros BT, Corr SJ, et al. (2013). Tumor selective hyperthermia induced by short-wave capacitively-coupled RF electric fields. *PLoS One* 8:e68506.
- [51] Pennes HH. (1948). Analysis of tissue and arterial blood temperatures in the resting human forearm. *J Appl Physiol* 1:93–122.
- [52] Yuan Y, Cheng KS, Craciunescu OI, et al. (2012). Utility of treatment planning for thermochemotherapy treatment of nonmuscle invasive bladder carcinoma. *Med Phys* 39:1170–81.
- [53] Oleson JR, Samulski TV, Leopold KA, et al. (1993). Sensitivity of hyperthermia trial outcomes to temperature and time: implications for thermal goals of treatment. *Int J Radiat Oncol Biol Phys* 25:289–97.
- [54] Dewhirst MW, Vujaskovic Z, Jones E, et al. (2005). Re-setting the biologic rationale for thermal therapy. *Int J Hyperthermia* 21:779–90.
- [55] Van Haaren PM, Hulshof MC, Kok HP, et al. (2008). Relation between body size and temperatures during locoregional hyperthermia of oesophageal cancer patients. *Int J Hyperthermia* 24:663–74.
- [56] Rhee JG, Lee CK, Osborn J, et al. (1991). Precooling prevents overheating of subcutaneous fat in the use of RF capacitive heating. *Int J Radiat Oncol Biol Phys* 20:1009–15.
- [57] van Rhoon GC, van der Zee J, Broekmeyer-Reurink MP, et al. (1992). Radiofrequency capacitive heating of deep-seated tumours using pre-cooling of the subcutaneous tissues: results on thermometry in Dutch patients. *Int J Hyperthermia* 8:843–54.
- [58] Kroeze H, van de Kamer JB, De Leeuw AAC, et al. (2001). Regional hyperthermia applicator design using FDTD modelling. *Phys Med Biol* 46:1919–35.
- [59] de Bruijne M, Wielheesen DH, Van der Zee J, et al. (2007). Benefits of superficial hyperthermia treatment planning: five case studies. *Int J Hyperthermia* 23:417–29.
- [60] Paulides MM, Stauffer PR, Neufeld E, et al. (2013). Simulation techniques in hyperthermia treatment planning. *Int J Hyperthermia* 29:346–57.
- [61] Erdmann B, Lang J, Seebass M. (1998). Optimization of temperature distributions for regional hyperthermia based on a nonlinear heat transfer model. *Ann N Y Acad Sci* 858:36–46.
- [62] De Greef M, Kok HP, Correia D, et al. (2011). Uncertainty in hyperthermia treatment planning: the need for robust system design. *Phys Med Biol* 56:3233–50.
- [63] Drizdal T, Paulides MM, van Holthe N, et al. (2017). Hyperthermia treatment planning guided applicator selection for sub-superficial head and neck tumors heating. *Int J Hyperthermia*. [Epub ahead of print]. DOI:[10.1080/02656736.2017.1383517](https://doi.org/10.1080/02656736.2017.1383517)
- [64] Sreenivasa G, Gellermann J, Rau B, et al. (2003). Clinical use of the hyperthermia treatment planning system HyperPlan to predict effectiveness and toxicity. *Int J Radiat Oncol Biol Phys* 55:407–19.
- [65] Kok HP, Korshuize - van Straten L, Bakker A, et al. (2017). On-line adaptive hyperthermia treatment planning during locoregional heating to suppress treatment limiting hot spots. *Int J Radiat Oncol Biol Phys* 99:1039–47.
- [66] Kok HP, Ciampa S, De Kroon-Oldenhof R, et al. (2014). Toward on-line adaptive hyperthermia treatment planning: correlation between measured and simulated specific absorption rate changes caused by phase steering in patients. *Int J Radiat Oncol Biol Phys* 90:438–45.
- [67] Kok HP, Korshuize-van Straten L, Bakker A, et al. (2017). Feasibility of on-line temperature-based hyperthermia treatment planning to improve tumour temperatures during locoregional hyperthermia. *Int J Hyperthermia*. [Epub ahead of print]. DOI:[10.1080/02656736.2017.1400120](https://doi.org/10.1080/02656736.2017.1400120)
- [68] ALBA. (2017). www.albahyperthermia.com.
- [69] Schneider CJ, van Dijk JD, De Leeuw AA, et al. (1994). Quality assurance in various radiative hyperthermia systems applying a phantom with LED matrix. *Int J Hyperthermia* 10:733–47.
- [70] Sahinbas H, Rosch M, Demiray M. (2017). Temperature measurements in a capacitive system of deep loco-regional hyperthermia. *Electromagn Biol Med* 36:248–58.
- [71] Harima Y, Nagata K, Harima K, et al. (2001). A randomized clinical trial of radiation therapy versus thermoradiotherapy in stage IIIB cervical carcinoma. *Int J Hyperthermia* 17:97–105.
- [72] Kouloulas VE, Kouvaris JR, Nikita KS, et al. (2002). Intraoperative hyperthermia in conjunction with multi-schedule chemotherapy (pre-, intra- and post-operative), by-pass surgery, and post-operative radiotherapy for the management of unresectable pancreatic adenocarcinoma. *Int J Hyperthermia* 18:233–52.
- [73] Kouloulas VE, Nikita KS, Kouvaris JR, et al. (2002). Intraoperative hyperthermia and chemoradiotherapy for inoperable pancreatic carcinoma. *Eur J Cancer Care (Engl)* 11:100–7.
- [74] Yamada S, Takai Y, Nemoto K, et al. (1992). Intraoperative radiation therapy combined with hyperthermia against pancreatic carcinoma. *Tohoku J Exp Med* 166:395–401.
- [75] Masunaga S, Hiraoka M, Takahashi M, et al. (1990). Clinical results of thermoradiotherapy for locally advanced and/or recurrent breast cancer-comparison of results with radiotherapy alone. *Int J Hyperthermia* 6:487–97.
- [76] Huilgol NG, Gupta S, Dixit R. (2010). Chemoradiation with hyperthermia in the treatment of head and neck cancer. *Int J Hyperthermia* 26:21–5.
- [77] Li G, Mitsumori M, Ogura M, et al. (2004). Local hyperthermia combined with external irradiation for regional recurrent breast carcinoma. *Int J Clin Oncol* 9:179–83.
- [78] Van Wieringen N, Wiersma J, Zum Vörde Sive Vörding PJ, et al. (2009). Characteristics and performance evaluation of the capacitive contact flexible microstrip applicator operating at 70 MHz for external hyperthermia. *Int J Hyperthermia* 25:542–53.
- [79] de Bruijne M, van der Holt B, van Rhoon GC, et al. (2010). Evaluation of CEM43 degrees CT90 thermal dose in superficial hyperthermia: a retrospective analysis. *Strahlenther Onkol* 186:436–43.
- [80] Sherar M, Liu FF, Pintilie M, et al. (1997). Relationship between thermal dose and outcome in thermoradiotherapy treatments for superficial recurrences of breast cancer: data from a phase III trial. *Int J Radiat Oncol Biol Phys* 39:371–80.
- [81] Leopold KA, Dewhirst MW, Samulski TV, et al. (1993). Cumulative minutes with T(90) greater than Tempindex is predictive of response of superficial malignancies to hyperthermia and radiation. *Int J Radiat Oncol Biol Phys* 25:841–7.
- [82] Hand JW, Lagendijk JJ, Bach Andersen J, et al. (1989). Quality assurance guidelines for ESHO protocols. *Int J Hyperthermia* 5:421–8.
- [83] Yee KS. (1966). Numerical solution of initial boundary value problems involving Maxwell's equations in isotropic media. *IEEE Trans Antennas Propag* 14:302–7.